NTNU – Trondheim
Norwegian University of
Science and Technology

High Temperature Decomposition of Methane on Quartz Pellets

Henrik Lindgaard

MSc in Physics
Submission date: June 2015
Supervisor: John Walmsley, IFY
Co-supervisor: Halvor Dalaker, Sintef

Norwegian University of Science and Technology
Department of Physics

Abstract

This work has shown that pure methane, when exposed to quartz at a temperatures of 900°C and 1000°C, cracks and deposits carbon at a near constant rate. The deposition rates for the individual temperature levels were shown to differ by a factor of approximately 7, where experiments at 1000°C showed the highest rate of deposition and those at 900°C the lowest.

The surfaces of the samples showed a definite increase after the treatment. While not definite, there were signs that surface area could be a function of deposited carbon mass.

There were not observed any weight increase on the sample treated at 700°C, and only small amounts on the sample at 800°C, indicating a cut-off temperature for the reaction in this

Contents

Chapter 1
Introduction

This study was motivated by a wish for increased knowledge of the mechanisms that control carbon deposition on quartz from the cracking of methane, a process which could contribute to reduced greenhouse gas emissions and higher efficiency in silicon production.

The demand for silicon is growing as it end uses - to a large extent as a reinforcing element in strong aluminium alloys and solar cells - are becoming ever more popular. As the silicon industry grows, so does its importance as an energy consumer and an emitter of greenhouse gases. This sets the stage for more research on possible improvements of the silicon production process in the years to come, wherein one promising avenue is the use of natural gas.

1.1 Silicon metal - Uses and trends

Silicon is available with varying purities and alloying elements, and the higher purities of silicon are often classified by *silicon metal* (>95 wt-% Si), *metallurgical grade silicon* (>98-99 wt-% Si), *solar grade silicon* (>99.9999 wt-% Si) and *electronic grade silicon* (>99.9999999 wt-% Si).

Silicon metal has its main use as an alloying element, providing tougher and more resilient aluminium alloys largely used in the car and construction industries. The second biggest consumer of silicon metal is the chemical industry, where it is used in the production of silicones which have a wide range of applications, such as gaskets, lubricants and sealants. Silicon metal or metallurgical grade silicon can also be upgraded and refined to produce high purities such as solar grade and electronic grade silicon, which is used for the production of solar cells and electronic devices respectively.

There has been a rise in silicon metal production during the past decades, as can be seen in figure 1.1, largely as a result of higher demand for strong aluminum alloys

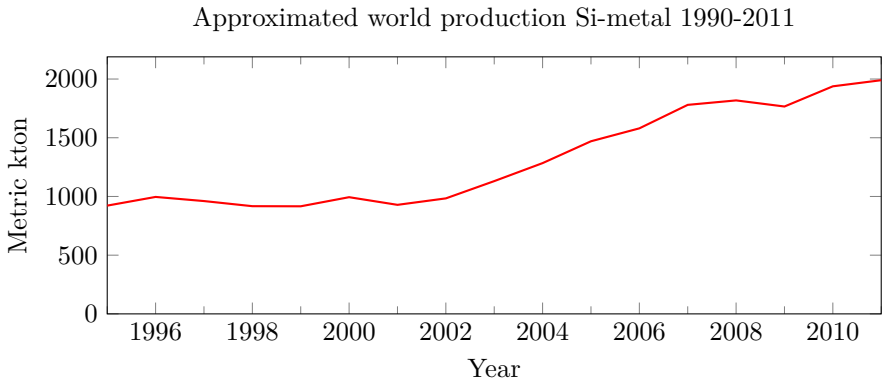

Figure 1.1: Approximated global silicon metal production by year. The figure shows a steady rise and near doubling during the period 2001 to 2011. The reader should note that values are based on the assumption that silicon metal represents a steady 80 wt-% of all embedded silicon of the compounded category *ferrosilicon and silicon metal* from the U.S. Geological Survey's *Mineral Commodity Summaries* on *Silicon* for the years from 1996 to 2014[1].

and a growing solar industry. It is fair to expect a steady rise in demand in the decades to come, making the production of silicon metal - and its environmental and energy considerations - an increasingly important subject.

1.2 Greenhouse gas emissions in silicon production

The production of 1 kg silicon metal in a submerged arc furnace, which is the main production process for silicon, emits around 6.1-6.5 kg of CO_2[2, 3]. While the majority of carbon comes from coal and coke, an approximately 30 % is supplied from renewable sources such as wood chips and charcoal [2, p. 324]. These numbers, however, do not account for any indirect emissions, such as fossil based electricity production, the production of coke and other upstream processes.

A purely theoretical limit[1] for the silicon furnace is approximately 3.13 kg of of CO_2 per kg of silicon metal produced, about half of that reported. While one could not expect to approach this limit, it still serves as an indication of the losses from the silicon production process.

1.3 Carbon in primary metal production

Carbon based or *carbonaceous* compounds, such as coal, coke and wood, play an integral part in the production of metal from ore, or *primary metal production*, both

[1]Calculations based on equation 1.1, assuming CO(g) reacting with O_2(g) to produce CO_2(g) (44.01 g/mol) with a ratio 2:1 for every Si(s)(28.09 g/mol) produced.

providing heat through combustion as well as beneficial chemical reactions. Its The choice of carbonaceous compound impacts the chemical reaction efficiency - and in turn - the CO_2-output for an amount of heat or metal produced. Stricter regulations and rising costs on greenhouse gas emissions have led to an intensification of research on production efficiency and the transition to less CO_2-intensive carbon sources.

1.4 Methane and silicon production

Silicon is produced by reacting silicon dioxide (SiO_2) with carbon at temperatures around 2000°C in large submerged arc furnaces. The raw material for SiO_2 is quartz, a crystal which makes up ∼50 wt-% of the earth's crust[4], while carbon typically is provided by a mix of coke, coal, charcoal and wood chips. One possible use of methane could be as a source of carbon[5], where it could work as a substitute for the conventional sources. This could lead to an overall reduction in greenhouse gas emissions, as coke have large CO_2-emissions associated with its production.

When substituting the regular sources, carbon deposited from methane, which is the main component of natural gas, could also contribute to a cleaner silicon metal, as it would have less impurities that could be carried on to the end product.

While there are is a lot of different chemical reactions present in the submerged arc furnace, the overall reaction is usually described by:

$$\mathrm{SiO_2}(\mathit{molten}) + 2\mathrm{C}(\mathit{solid}) \rightleftarrows \mathrm{Si}(\mathit{molten}) + 2\mathrm{CO}(\mathit{gas}) \tag{1.1}$$

This reaction happens in the hottest part of the furnace, and creates a dome from the pressure of generated CO gas. The majority of gas present is a mix of CO(g) and SiO(g), and as the pressure builds, the gases will start to vent in a steady flow. As the gas is escaping through the upper layers of the furnace, some SiO(g) reacts with carbon and oxygen and deposits as SiC(s) and SiO_2(s). However, a significant amount of SiO(g) escapes from the furnace altogether, which constitutes both a loss of heat and of chemical reaction energy - a loss, which together with CO(g), CO_2(s) and H_2O(g), represents approximately 50 % of the energy input as shown in figure 1.2. Wherein lies the third possible advantage of introducing carbon deposited from methane in the silicon process, as it is speculated to have a high reactivity with SiO(g), thus reducing its losses through the furnace off-gas.

1.5 Objective of this thesis

It may be apparent from the previous sections that silicon metal production is becoming an increasingly important topic. The production volume is increasing, as is the benefits and disadvantages. More silicon means more solar cells and lighter cars, but it also represents energy expenditure and environmental costs. Research on

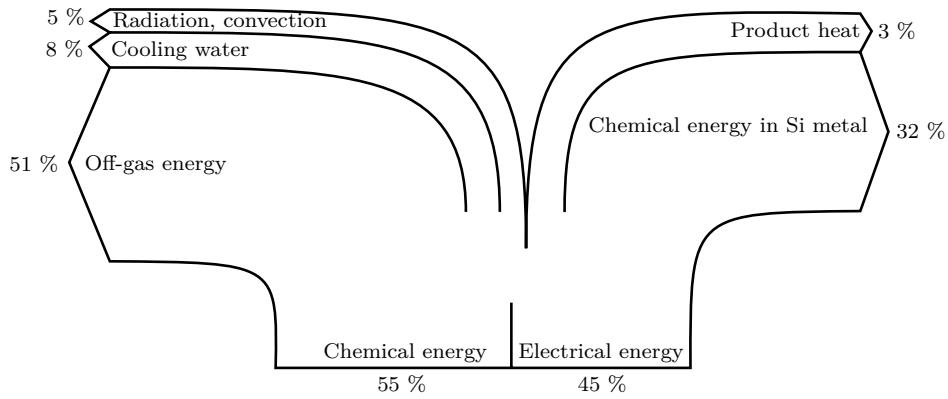

Figure 1.2: The energy inputs and outputs in typical silicon metal production (*adapted from* Tuset et al. [2]). One should note that only 32 % of the energy input ends up in the metal.

increasing the efficiency and reducing the impacts of silicon metal production will only become more and more important as its use continues to grow.

Methane could prove to be a significant contribution in production of silicon, with the potential to both serve as a pure source for carbon and help reduce losses. This would be precluded by understanding how one treats the methane to make use of its carbon, and subsequently, by determining how it will work in practice.

The important contributions that could be made from this study, were related to the use of methane as a source for carbon deposited on quartz. To get increased knowledge of this process, factors such as deposition rates and surface structure were to be examined - possibly contributing to a better understanding of how the reaction takes place.

This study could contribute to the basic knowledge on the deposition of carbon from methane on quartz, and while only being part of the initial efforts on the subject, it constitutes a crucial step towards a final industrial application.

1.6 Thesis outline

In the following chapter the reader will be given some introductory knowledge of *state of the art* silicon production. This will be done by providing some background on the chemical reactions which makes carbon such an integral part of metal production, before moving on to some specifics on silicon.

As there is scarce research on the use of methane in silicon production, the theory chapter will mainly offer some information on related research.

After a short description of the equipment used, the reader will be given an extensive summary on the experimental procedure. The final parts of the method will provide some information on the choice of samples, treatments and analysis.

Observations made as part of the experimental treatment procedure will be presented in its entirety (if available), as will data from later surface analysis. At the end of chapter 5, the reader can observe a small selection of images showing the type of information that was available from the scanning electron microscope sessions.

The most evident observations will be interpreted in chapter 6 and some of the observations will be discussed. This is followed by some reflections on which mechanisms may control the deposition process, how they would manifest themselves and if they appear in the data.

While this work has presented new knowledge, it has also given rise to new questions and the need for additional data. Ahead of the concluding remarks, in chapter 7, the reader will be presented with suggestions for future research.

At the end of this thesis, the knowledge gained from this work will be summed up with a focus on the well founded conclusions.

Chapter 2
Background

A majority of today's metals are produced by the help of carbon as chemical reactant. Together with its origin, be it fossil or renewable, the efficiency at which the carbon is utilized is of major importance. This chapter tries to give the reader an introductory knowledge of the production of metals from metal oxides by the use of carbon, and finally, its role in silicon metal production.

2.1 Primary metal production

While it is assumed that the reader has a basic understanding of the chemistry and thermodynamics included in this thesis, section 2.1 will offer some brief descriptions on subjects such as *Gibbs free energy* and *chemical equilibria* in order for the reader to touch up on, and have these concepts fresh in mind, for the following subject matter. However, a comprehensive description of the chemistry and physics involved in the reduction of metal oxides is beyond the scope of this thesis, and for inquisitive readers - as well as readers which find some of the simplifications or visualizations hard to follow - the author recommends the book *Chemical Thermodynamics of Materials: Macroscopic and Microscopic aspects* by Stölen and Grande [6], a book from which the a substantial part of the following sections are derived.

2.1.1 Reduction-oxidation reactions

Reduction-oxidation reactions are chemical reaction in which atoms change their *oxidation state*. The term oxidation state describes the number of electrons in an electron shell of a particular atom, relative to its neutral state. Being negative, an electron surplus correspond to a negative oxidation state, while a loss of electrons gives a positive oxidation state. As a rudimentary illustration, figure 2.1 shows a (*non-stoichiometric*) reaction in which chlorine gas reacts with sodium to form regular table salt.

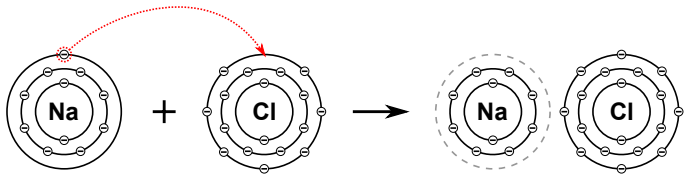

Figure 2.1: Illustration of the loss (*or oxidation*) of sodium and gain of electrons (*or reduction*) of chlorine as Na and Cl reacts.

At the outset, both sodium and chlorine are neutral atoms, having a number of electrons which corresponds to their core charge (Cl^0 & Na^0). However, as a reduction-oxidation reaction take place, chlorine - having a higher affinity for electrons - attains a surplus of electrons, while sodium loses one electron. Although the resulting molecule is neutral, sodium now has an oxidation state of +1 (Na^{+1}) and chlorine has an oxidation state of -1 (Cl^{-1}). We can say that, as a result of the reaction, sodium has *oxidized* and chlorine has been *reduced*. In a similar manner, one can also say that chlorine has oxidized sodium, and that sodium has reduced chlorine.

While the terms reduced and oxidized are relative terms, by which it can be hard to infer the initial and final molecular structure of a reaction - one should take the term *reduced/reduction of a [metal oxide]*, if not else specified, to mean the reduction of a metal to its pure neutral state.

2.1.2 Gibbs free energy

For systems kept at constant temperature and pressure, *Gibbs free energy* consolidates the two main properties in thermodynamics into a single quantity, G:

$$G = H - TS \tag{2.1}$$

Here, the letter H represent enthalpy, S entropy and T is the temperature of the system. Thermodynamic systems tend toward:

1. **Dissipation of energy *or* loss of *enthalpy* (H)**
   Enthalpy is the *thermodynamic potential* of a system, and can be viewed as a potential energy which can be exchanged between the system and its surroundings, either by pressure or heat. In processes where temperature and pressure are kept constant, this potential energy exchange consists of the system releasing og absorbing heat.
2. **Increased disorder *or* increased *entropy* (S)**
   Entropy is a measure of the disorder of a system, and is probably best understood by attaching real-world examples to the term. A popular example is that of regular water (H_2O) and its different phases - ice, liquid and gas. When

present as ice, H_2O is highly organized and structured in a crystal lattice, which correspond to a low entropy. If melted, ice would lose its crystal structure, and while forces between the individual H_2O molecules would still keep it somewhat connected and organized, it would be less organized than ice and have a higher disorder. By boiling water, one would release the individual water molecules into the air as a gas, becoming less organized than both ice and water, and having the highest disorder and entropy of the three phases.

Concerning chemical reactions, the main point of interest is the change of Gibbs free energy or the *Gibbs free energy of reaction ($\Delta_r G$)*:

$$\Delta_r \mathrm{G} = \Delta_r \mathrm{H} - \mathrm{T}\Delta_r \mathrm{S} \tag{2.2}$$

While enthalpy tends towards dissipating energy and entropy tends towards increased disorder, a chemical reaction tends towards a negative Δ_rG - a somewhat optimal compromise between reduced H and increased S. In reactions where Gibbs energy of reaction is negative, one can say that the reaction is thermodynamically favored or *spontaneous*[1]. Correspondingly, reactions which have a positive Gibbs energy of formation are called *non-spontaneous*.

2.1.3 Chemical Equilibrium

When trying to understand chemical reactions, it is important to avoid visualizing transitions between two static states. A more helpful image would be that of randomly mixing reactants and favorable collisions, where by chance, chemical products are being created in a dynamically changing system.

One can divide chemical reactions into *reversible* or *irreversible*. While reversible reactions can proceed in both directions, irreversible reactions only proceed in one direction. As an irreversible reaction exhausts the available reactants, favorable collisions become less and less likely - the rate of conversion slows off until, finally, one of the reactants are depleted and no new products are created.

Reversible reactions, like irreversible reactions, rely on random collisions between reactants to form a product - however, as opposed to irreversible reactions, random collisions between the products may also recreate the reactants - i.e. the reaction can and will proceed in the reverse direction. The differences can be summarized by the following equations:

[1] One should note that the term *spontaneous* in chemistry neither describes the rate of nor if a reaction is going to happen, but rather tells if a reaction is thermodynamically favorable.

For irreversible reactions

$$\mathrm{A} + \mathrm{B} \rightarrow \mathrm{C} + \mathrm{D} \tag{2.3}$$
$$\mathrm{C} + \mathrm{D} \nrightarrow \mathrm{A} + \mathrm{B} \tag{2.4}$$

For reversible reactions

$$\mathrm{A} + \mathrm{B} \rightarrow \mathrm{C} + \mathrm{D} \tag{2.5}$$
$$\mathrm{C} + \mathrm{D} \rightarrow \mathrm{A} + \mathrm{B} \tag{2.6}$$

When dealing with *chemical equilibrium*, only reversible reactions are of interest. As mentioned, collisions between reactants and collisions between the products impact the forward and backward rates of reaction. While a reaction may strongly favor going in the forward direction, as the reactants are depleted, favorable collisions between the reactants become less and less likely. At the same time, the fraction of colliding products gets higher and higher and - even though the backward reaction is much less favored - the sheer amount of collisions leads to a higher rate of the backward reaction. At a specific distribution between the reactants and products, both the forward and backward rates of reaction are equal, the concentrations stops changing and the reaction is at chemical equilibrium.

The equilibrium of a reversible reaction is related to Gibbs free energy of the reaction by the following equation:

$$\Delta_r \mathrm{G}^o = -RT \ln K_{eq} \tag{2.7}$$

Here $\Delta_r \mathrm{G}^o$ is the change of Gibbs free energy for the reaction, R is the gas constant and T is the temperature of the system. The last factor is K_{eq}, which represents the ratio between the reactants and the products. Based on a hypothetical reaction:

$$\alpha\mathrm{A} + \beta\mathrm{B} + \ldots \rightleftharpoons \sigma\mathrm{C} + \tau\mathrm{D} + \ldots \quad , \tag{2.8}$$

and where there are some species A, B and so on, reacting and turning into C, D, ... – where α, β, σ and τ describe the stoichiometrics of the reaction – the equilibrium constant can be defined as:

$$K_{eq} \equiv \frac{a_C^{\sigma} a_D^{\tau} \cdots}{a_A^{\alpha} a_B^{\beta} \cdots} \tag{2.9}$$

Here the a represents the effective concentrations or thermodynamic *activities* of the different species. Generally, one can say that the activity of a species describes how available it is for favorable collisions. Although one species may interact with other species present, making it more or less available for favorable collisions, such

distinctions are not important in this subject matter. By assuming ideality, the activities of solids and liquids equal their molar fractions, and gases are reduced to their partial atmospheric pressure.

$$\Delta_r \mathrm{G}^o = \overbrace{(\sigma \Delta \mathrm{G}^o_C + \tau \Delta \mathrm{G}^o_D + \ldots)}^{products} - \overbrace{(\alpha \Delta \mathrm{G}^o_A + \beta \Delta \mathrm{G}^o_B + \ldots)}^{reactants} \tag{2.10}$$

By rewriting equation 2.7, it becomes obvious that if we know the Gibbs free energies of the reacting species, we know something of their distribution at equilibrium:

$$\frac{a^\sigma_C a^\tau_D \cdots}{a^\alpha_A a^\beta_B \cdots} \equiv K_{eq} = e^{-\Delta_r \mathrm{G}^o / RT} \tag{2.11}$$

If the Gibbs energy of reaction has a large negative value, the exponential function in 2.11 becomes large, which implies that a equilibrium is product favored:

$$a^\sigma_C a^\tau_D \ldots \gg a^\alpha_A a^\beta_B \ldots \qquad \Delta_r \mathrm{G}^o \ll 0 \tag{2.12}$$

Similarly, a very high positive free energy of the reaction, implies the opposite:

$$a^\sigma_C a^\tau_D \ldots \ll a^\alpha_A a^\beta_B \ldots \qquad \Delta_r \mathrm{G}^o \gg 0 \tag{2.13}$$

And finally, if there is no change in free energy:

$$a^\sigma_C a^\tau_D \ldots = a^\alpha_A a^\beta_B \ldots \qquad \Delta_r \mathrm{G}^o = 0 \tag{2.14}$$

2.1.4 Reduction of metal oxides

Most metals, with the exception of gold and platinum - and to a smaller extent, copper and silver - do not occur as pure metals in the earths crust [REF]. This is a result of different metals tendency to chemically react with periodic elements such as sulfur and oxygen, forming molecules such as Fe_2O_3, As_2S_3 and SnO_2 - and compounds such as CO_2 which, when dissolved in water, reacts and form carbonates (e.g. $CaCO_3$,$ZnCO_3$ and $MgCO_3$,). Based on a desired metal product, one has to start with a corresponding metal containing ore found in nature and, through engineered processes, remove the chemically bound oxidizing atoms or molecules, such as oxygen, sulfur and carbonate.

To remove the oxygen from or *reduce* a metal oxide, one usually has to find a competing oxidation reaction which produces a more stable oxide - i.e. another element or molecule with a greater affinity for oxygen than the desired metal. An often used tool to illustrate the stability of different oxides is an *Ellingham diagram*[7], as shown in figure 2.2. These diagrams show the *Gibbs free energy* of oxidation reactions with respect to temperature. The values are normalized to one mole of

O_2 reacting, and partial gaseous pressures and pressure ratios are all set to unity ($P_{O_2} = P_{H_2}/P_{H_2O} = P_{CO}/P_{CO_2} = 1$).

As shown earlier, reactions with large negative Gibbs free energies react to produce stable compounds - the larger the negative value, the more tightly bound and less reactive the product. By looking at figure 2.2, some of the metal oxides which are hardest to reduce are magnesia and alumina. As alumina is placed slightly lower on the diagram one may conclude that aluminum has a greater affinity for oxygen than magnesium - i.e. aluminum could be used as a reducing agent for magnesium oxide under the right conditions. While this reaction is in fact feasible, the cost of aluminum consumed outweighs the potential value of magnesium produced, making such a reaction economically unsound.

While the Ellingham diagram in figure 2.2 gives a good indication of which reactions are likely to take place under somewhat standard conditions, the drawing of Ellingham diagrams was quickly expanded upon by Richardson and Jeffes [8] to account for varying partial pressures. As discussed in section 2.1.3, when an equilibrium is attained there will be a certain ratio between the reactants and products. If one partially remove or add one of the species taking part in the reaction, the rates at which the reaction proceeds in both directions will change until a new equilibrium is achieved. If one continuously removes one of the species, such as evacuating O_2 gas by vacuum, oxidation reactions which usually are favored in the forward direction could be reversed. One example of such a vacuum reduction reaction is that of copper:

$$4\mathrm{Cu(s)} + \mathrm{O_2(g)} \rightleftharpoons 2\mathrm{Cu_2O(s)} \tag{2.15}$$

$$2\mathrm{Cu_2O(s)} + \mathrm{O_2(g)} \rightleftharpoons 4\mathrm{CuO(s)}, \tag{2.16}$$

As demonstrated by Lee et al. [9] at pressures below $1{\cdot}10^{-5}$ Pa, CuO(s) will be almost completely reduced to Cu_2O(s) following the reverse of reaction 2.16 at 400°C, at which point copper metal will begin to form from the reverse of reaction 2.15.

A *Richardson-Ellingham diagram*, which has been expanded to take account for these effects in pressure, is depicted in figure 2.3 and shows three *nomographic* scales extending from the bottom left to the top right part of the diagram. These scales were added to both show the reductive powers of CO and H_2 with varying partial pressure ratios, as well as illustrate changes in the Gibbs free energy of formation for the metal oxides themselves oxygen pressure varies.

One should note that Gibbs free energy of a reaction is not the only factor determining if and how a reaction will proceed, and both *activation energies* and *reaction kinetics* would have to be considered in a real world case.

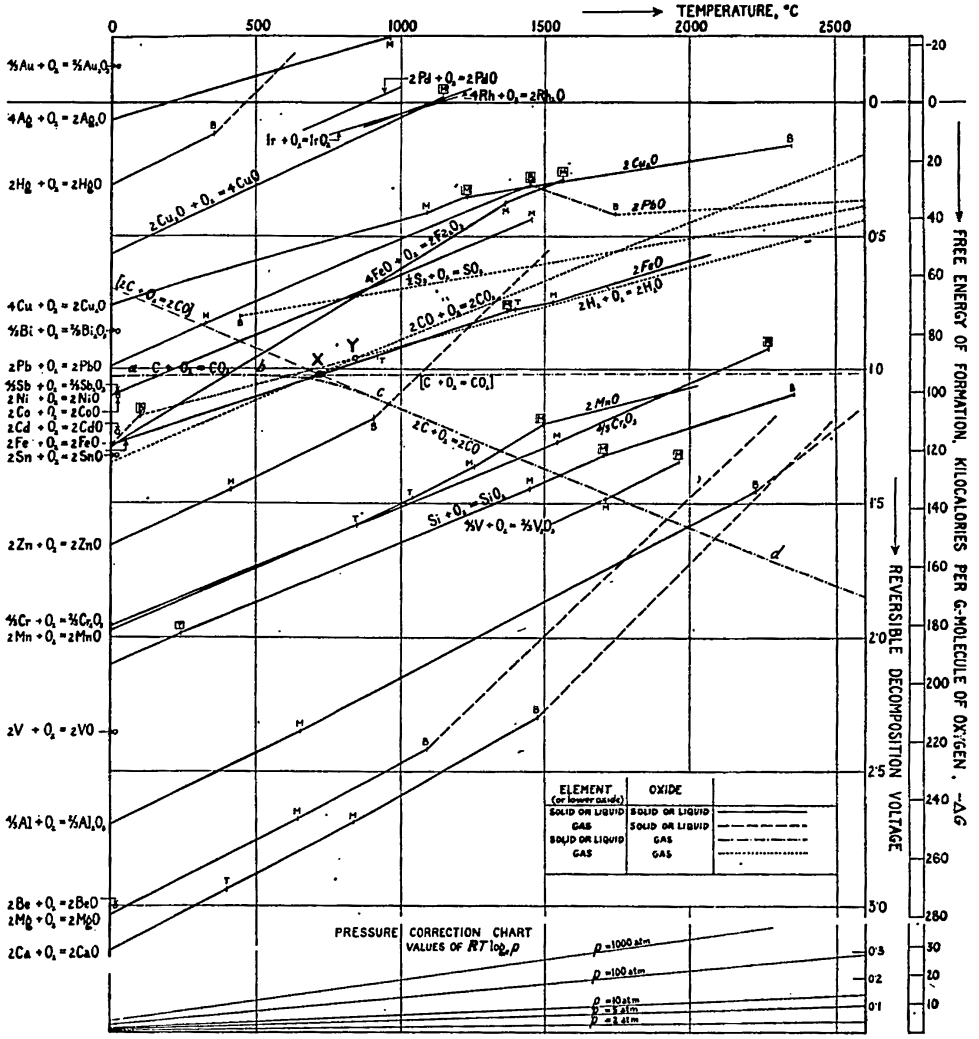

Figure 2.2: The above image is a screen capture from Harold Johann Thomas Ellingham's original article in the Journal of the Society of Chemical Industry from 1944 [7], which was to become a blueprint the analytical tool now known as just *Ellingham diagrams*.

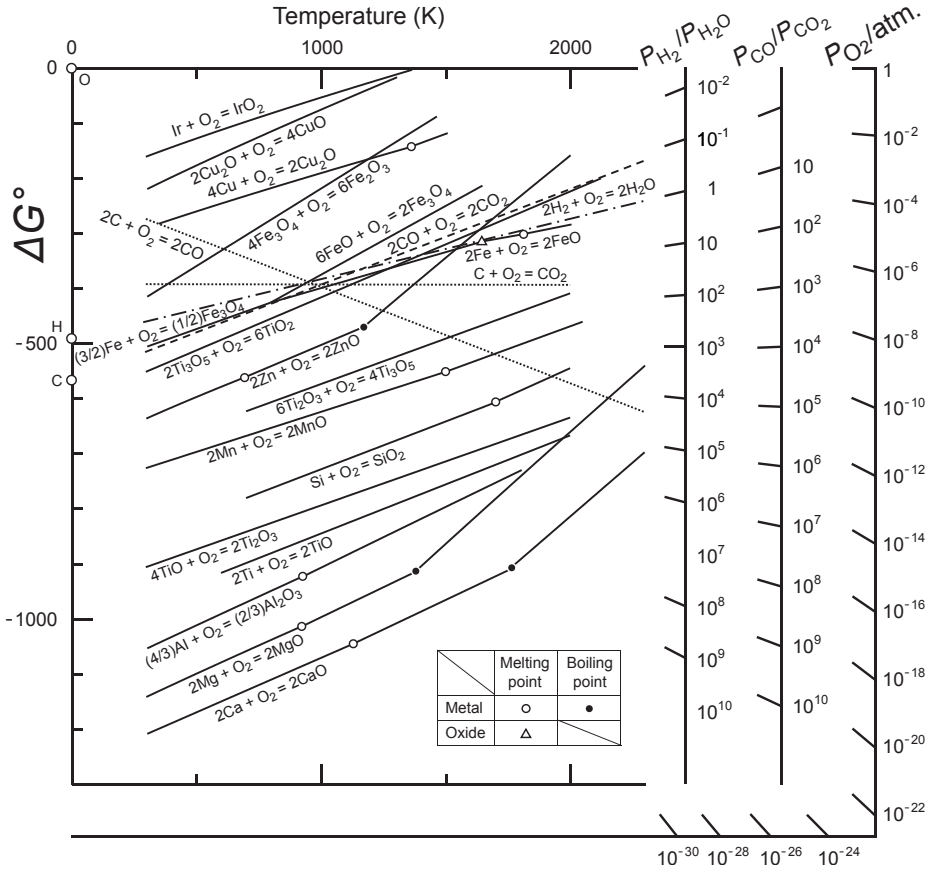

Figure 2.3: . . . nomographic . . .

2.1.5 Carbothermic reduction

Carbothermic or *carbothermal* is a combination of the words *carbon* and *thermal*, implying a processes in which both carbon and heat are present. In chemistry and materials technology the word is used to describe a processes that consist of heating a mix of metal oxides and carbon to produce pure (*or reduced*) metal.

To apply carbon as a reducing agent, one has to achieve temperatures at which the following reactions are more desirable than the desired metal oxide:

$$2\mathrm{C} + \mathrm{O_2} \rightleftharpoons 2\mathrm{CO} \tag{2.17}$$

$$\mathrm{C} + \mathrm{O_2} \rightleftharpoons \mathrm{CO_2} \tag{2.18}$$

Or indirectly from CO produced by reaction 2.17 or the Boudouard reaction which is favored in the forward direction for temperatures above 950°C:

$$C + CO_2 \rightleftharpoons 2CO \tag{2.19}$$

By looking at the Ellingham diagram in figure 2.3, both reactions 2.17 and 2.18 should be able to reduce the different iron oxides (Fe_2O_3, Fe_3O_4 and FeO) at temperatures exceeding 750-800°C. While this may be the case, both the iron oxides and carbon are solid at these temperatures, which precludes the vast majority of carbon and iron oxide from getting in direct contact. To increase the interactions between the reductant and the oxide, one either has to produce CO gas or increase the temperature until iron oxide melts at around 1500°C. This highlights the fact that free energy is not the only factor when identifying the viability of reduction reactions.

While the carbothermic reaction in theory can be used to reduce most of the metal oxides given a high enough temperature and, as discussed at the end of section 2.1.4, having the appropriate gas pressures, there is a limitation for its use in industrial scale operations, and e.g. aluminas and magnesias are not produced by this process. However, carbothermic reduction globally represents the biggest metal oxide reduction process as it is used in the production of iron and steel as well as the growing silicon metal production.

2.1.6 Silicon metal production

As briefly described in the introduction (chapter 1.4), silicon metal is produced by reacting SiO_2(s) with carbon at temperatures around ∼2000°C. The production takes place in large crucible shaped furnaces, as shown in figure 2.4(a) [2]. The carbothermic silicon process gets its heat from both electricity and chemical reactions, and its input is primarily a mix of quartz and carbonaceous sources. Given its fairly low placement in Ellingham diagram (figure 2.3), SiO_2(s) is one of the most stable and difficult to reduce metal oxides produced by the carbothermic process.

Electric heat is supplied by large carbon electrodes, where heat is evolved from resistance of the feed material as well as electric arcs passing through gaseous domes *or cavities* beneath the electrodes which are shown in figure 2.4. As metal oxide gets reduced, along with the other reactions taking place at the core of the silicon furnace, the carbon electrodes continually gets consumed. An example given by Tuset et al. [2, p. 178] estimates a ∼10 % carbon contribution to the chemical reactions from the the electrodes, with the remaining being provided by coal (∼70 %) and wood chips (∼70 %).

The selection of feed material for the silicon furnace has a significant impact on the purity of the end product, where impurities from both the quartz as well as the

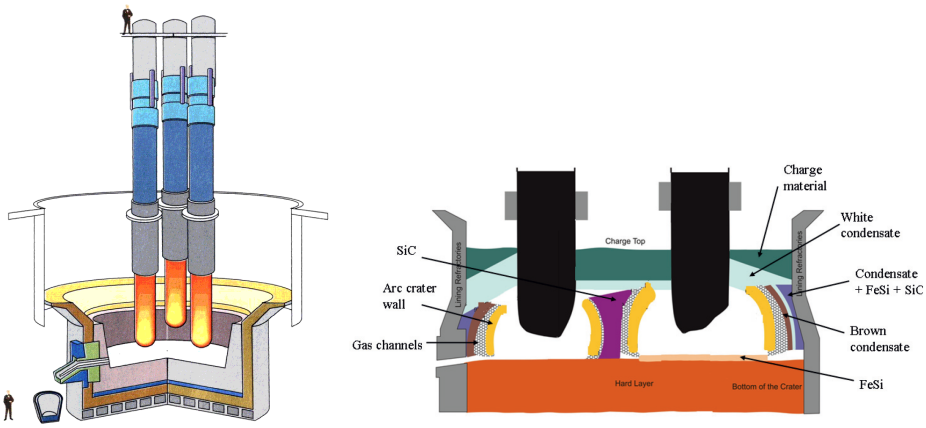

(a) Scaled image of a silicon furnace (b) Depiction of excavated ferrosilicon furnace

Figure 2.4: (a) To proivde an impression of the scale of the silicon furnace, an image from [2, p. 104] has been included, where one can se how the size of a human compares to the dimensions of the furnace. (b) An image showing the composition of different layers in an excavated ferrosilicon furnace. The main points are craters or *cavities* which can be view beneath the electrodes, as well as different arc crater wall - creating the chamber wherein the main reduction of silicon metal takes place - as illustrated in Martello [10].

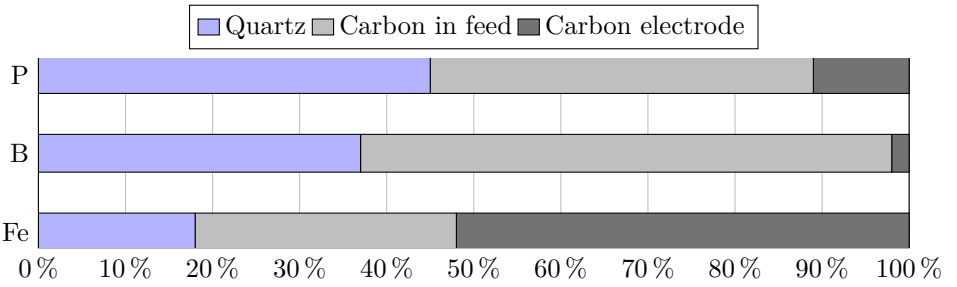

Figure 2.5: Sources for different impurities which ends up in the final silicon or ferrosilicon product, as adapted from by [11].

carbonaceous sources end up in the silicon metal produced. A typical distribution of sources of impurities in the silicon furnace is shown in figure 2.5.

The ability of carbon to reduce a particular metal oxide is closely related to both the metal's and carbon's affinity for oxygen. By looking at figure 2.3 and the line for $2C + O_2 = 2CO$, it is apparent that - as one moves down to the lower metal oxides - it becomes exceedingly difficult to utilize carbon as as a reducing agent. In addition, the equilibrium of *Boudouard reaction* (reaction 2.19), in which carbon dioxide consumes carbon to form carbon monoxide, limits the reductive properties of CO(g) at higher temperatures. This makes elemental carbon the main reducing

agent, earlier shown in reaction 2.17, giving the overall reduction to silicon metal:

$$SiO_2(l) + 2C(s) \rightleftarrows Si(l) + 2CO(g) \tag{2.20}$$

The actual chemical reactions taking place within the furnace are more complex than is evident from reaction 2.20. It consists of a set of different and interacting equilibrium reactions, being controlled by the partial pressures of gases, the solids that are present and the different temperatures which exsist throughout the silicon furnace. While it there is no need to delve into all the different reactions taking place, there are two reactions that are quite relevant to this thesis - the production of silicon metal and how carbon may play a role to reduce losses through the off-gas.

While reaction 2.20 often serves as an overall description reduction reactions of $SiO_2(s)$ to silicon metal, the final reaction steps to producing Si are between silicon carbide and SiO gas, as shown in figure 2.6:

$$SiO(g) + SiC(s) \rightleftarrows 2Si(l) + CO(g) \tag{2.21}$$

While, as also shown in the diagram, there are a lot of different reactions that create SiO gas, one should note that SiO a crucial and unavoidable compound in this reaction, as is carbon present in SiC(s).

A second important reaction is that of escaping SiO gas reacting with carbon[5]:

$$SiO(g) + 2C(s) \rightleftarrows SiC(s) + CO(g) \tag{2.22}$$

This reaction both produces SiC(s) which will be carried down through the furnace, as well as add heat, being a contributor to reducing the energy loss in the silicon furnace.

Since the loss of SiO gas will be mitigated by the reaction between SiO(g) and C(s), the reactivity towards SiO(g) gas is an important property of any carbonaceous material considered for Si production. The hypothesis that carbon from methane will have a very high reactivity towards SiO-gas is one of the main motivations behind the SiNG[2] project.

[2]SiNG is an abbreviation for *Silicon production with the use of Natural Gas* - a joint research project between SINTEF Materials and Chemistry and Elkem AS - which addresses the viability of introducing natural gas in Silicon production.

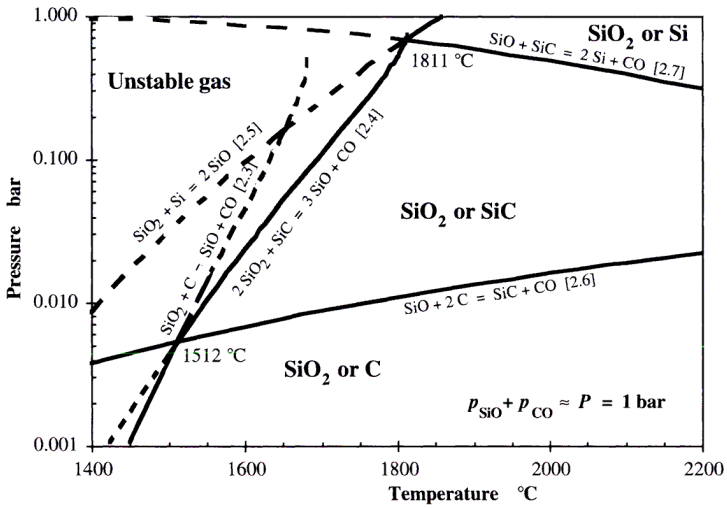

Figure 2.6: Equilibrium partial pressure of SiO gas as a function of temperature as provided in Tuset et al. [2, p. 29]. One should note that the final silicon producing step is a the reaction between SiO(g) and SiC(s), shown at the top right in the diagram (marked 2.7).

Chapter 3
Theory

As far as the author has been able to determine, not a lot of previous research has focused solely on the high temperature interactions between methane and SiO_2. As a result, this chapter will only make short descriptions of some related research.

3.1 Related research

3.1.1 Silica as catalyst support

While silica has been used extensively in research on the cracking of methane, as far as the author has been able to determine, its function has solely been as a support material for other more potent catalysts. One of the most comprehensive reviews of methane catalytic cracking have been made by Amin et al. [12].

3.1.2 Carbon black and activate carbon

Some of the more closely related research on the cracking of methane is based on *carbon blacks* and *activated carbon*. The former is a common denominator for high purity carbonaceous particulates while the latter describes a carbon material which has a very high specific surface area.

Initially, both carbon black and activated were considered as offering possible insight for this work. However, the bulk of the research on theses subjects, as related to this study, were mainly related to materials with a large surface area.

One group which has made several studies on carbon blacks as a catalyst for methane cracking are *Instituto de Carboquimica* in Spain. The common denominator for the work has been high surface areas, and in contrast to this work, a reduction of surface area throughout the deposition[13, 14, 15].

3.1.3 Direct use in metal production

At present, methane is already being applied as a reducing agent for iron oxides also known as the DRI process[16]. While reviewing the available literature on the subject, no articles focused on the deposition of carbon.

The most closely related work that was found, had been undertaken by Oleg Ostrovski[17] which had published several papers on the surface reactions of methane with different metal oxides. Although Ostrovski's work did have some common denominators with this work, it proved to be of little relevancy for this thesis.

3.1.4 Summary on literature

There were a lot of different articles and research touching on the subjects of this thesis, however, the conclusion were that this is a relatively new area within the production of metals.

3.2 Michaelis-Menten

While doing the final analysis in this thesis, the sample surfaces seemed to have a quick area increase during the initial phases before leveling out. This led to the use of a Michaelis-Menten equation, which is used to describe a completely different phenomenon, the kinetics of enzymes.

The reason for this choice was purely a of it providing a similar shape, which can be seen in figure 3.1

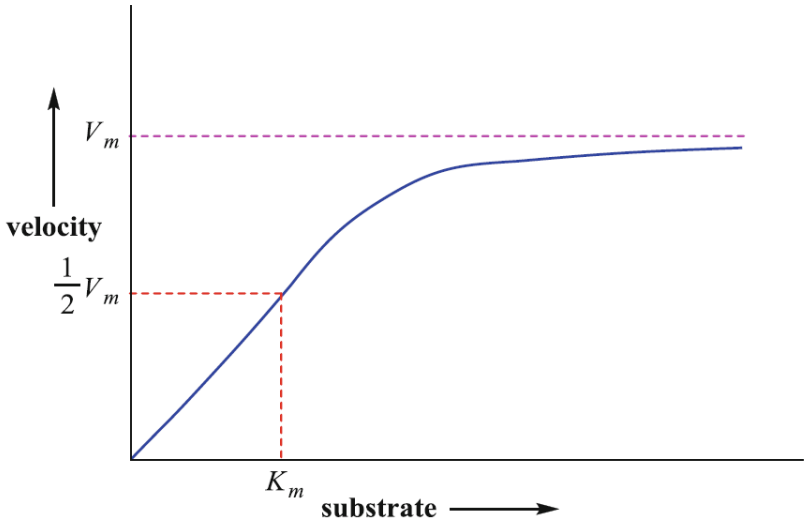

Figure 3.1: An example of the shape of a Michaelis-Menten function, showing an initial stable and rapid increase, before converging to specific value. Image is taken from Fromm and Hargrove [18].

Chapter 4
Method

Experimental work carried out during this study consisted of a series of 24 experiments, where samples composed of quartz were exposed to methane at elevated temperatures and different durations.

The following sections will give a detailed description of the experimental procedure, providing a reference for potential future work. In the concluding sections of this chapter, some information on choice of samples, treatments and analysis will be provided.

4.1 The experimental setup

The main objective of this research was to study the cracking of methane, and subsequent deposition of carbon, on quartz. In this respect one would need equipment in which quartz could be exposed to methane at high temperatures. In this respect the vertical tube furnace, as depicted in figure 4.1 was an appropriate choice.

Roughly speaking, the vertical tube furnace consists of a cylindrical hole surrounded by heating elements. This makes it possible to insert a tube going through the furnace, as illustrated by the *inner furnace tube* in figure 4.1. By attaching sealed caps with tubing at each end, one is able to pass different gases through the furnace while simultaneously providing heat.

Before proceeding with a descriptions of what influenced the choice of equipment, sample materials and treatment - a thorough description of the equipment and procedures used in the treatment of samples with methane gas will be given. This is done to enable easier reproduction of the experiments performed in this study, as well as provide a basis for comparison.

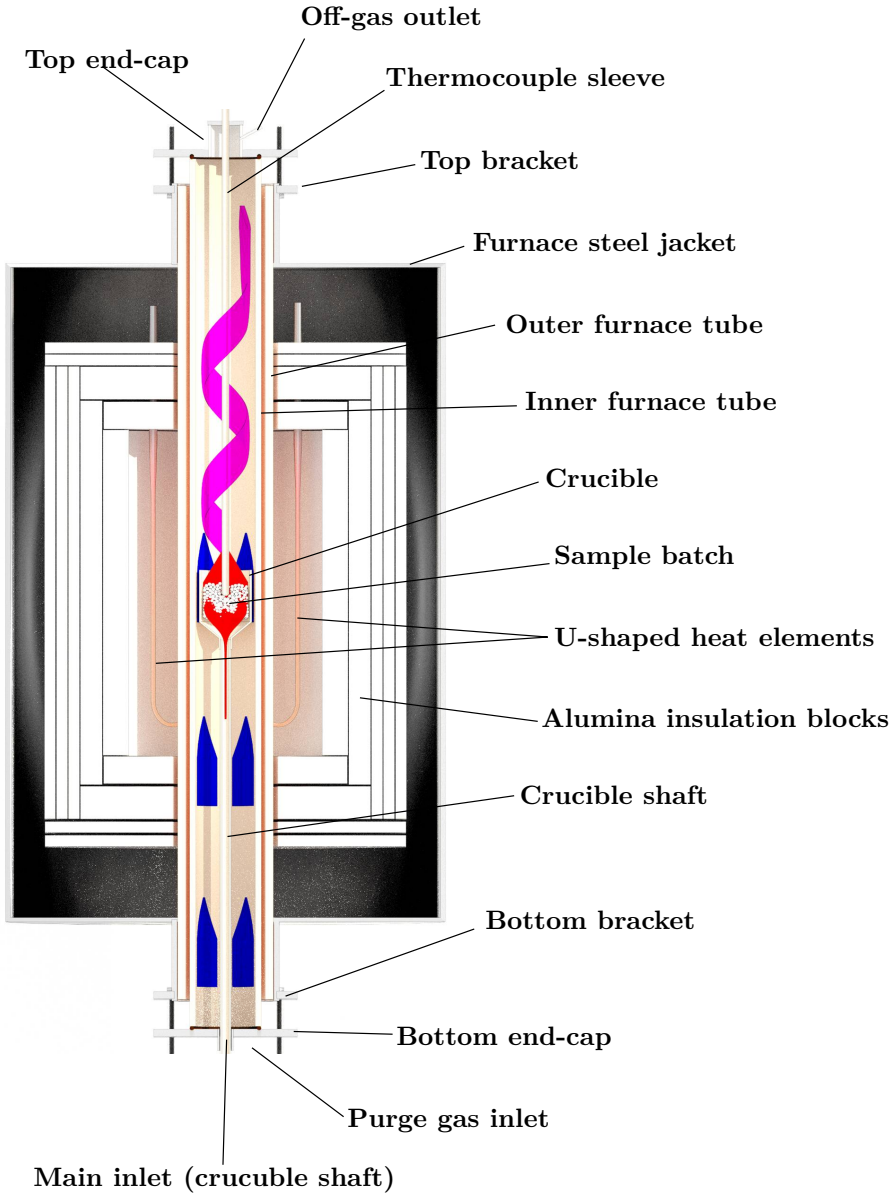

Figure 4.1: The above image illustrates a vertical cross section of the furnace setup used in the experiments. There are two different gas inlets at the bottom of the vertical tube furnace, the main gas inlet which provides gas flow through the crucible and sample batch, as illustrated with red. A second inlet, or *purge* gas inlet, is situated situated beside the main gas inlet, and its flow through the furnace is indicated by the blue arrows. In the area above the crucible, purge gas and main inlet gas will mix and ascend to the top of the inner furnace tube (purple) before it leaves the furnace through the off-gas outlet. Not shown in the illustration is the side mounted thermocouple that was used to control the furnace temperature.

4.2 Experimental treatment procedure

To better present how experimental procedure was prepared and performed, the following chapters will focus on individual stages separately. The overall structure of one individual experimental run consisted of the following steps:

1. **Partial assembly and equipment preparation**
   Partial assembly of the apparatus, cleaning of gaskets and non-removable surfaces, application of lubricant.
2. **Sample preparation**
   A sample batch exceeding 40 grams was transferred to the alumina crucible and the exact weight was recorded.
3. **Final assembly**
   Insertion of crucible, aligning and tightening of inner furnace tube end-caps, attaching gas-supply tube to crucible shaft.
4. **Initial gas flushing**
   Argon gas purge is initiated while monitoring integrity of the equipment. Brief methane flush followed by a switch to argon through the crucible shaft.
5. **Coolant check and heat schedule start**
   When methane from the short flush is expected to be displaced by argon, circulation of coolant is confirmed and heat schedule is set and initiated.
6. **Purge is suspended**
   After approximately 20 minutes, argon through purge inlet is suspended while argon through main inlet/crucible is maintained.
7. **Initial temperature stabilization**
   Wall set-point temperature is adjusted until a correct and stable temperature in the sample crucible is reached.
8. **Treatment start**
   Argon gas flow is stopped, methane gas is stepwise increased to 0.5 liter/min, time is noted down and personal gas detector is turned on.
9. **Treatment temperature stabilization**
   Temperature fluctuations are counteracted, seeking to attain stable target temperature
10. **Treatment stop**
    At the end of the scheduled time, methane gas flow is stopped and replaced with argon. Argon purge is reinitiated and the temperature program is stopped and furnace power switch is turned off.
11. **Cooling phase**
    After approximately 20 minutes, argon purge is discontinued. Argon flow

through crucible tube is reduced to 0.2 liter/min for the rest of the cooling period.

12. **Sample extraction and registration**
When at room temperature, the sample batch is extracted, weighed and transferred to marked zip-lock bags.

4.2.1 Partial assembly and equipment preparation

Before each run, all furnace parts which were going to be exposed to hot methane gas were cleaned. The removable inner alumina parts of the furnace, which consisted of the thermocouple sleeve, the inner furnace tube and the sample crucible and shaft (see figure 4.1) would have carbonaceous deposits from previous experimental runs. These deposits were removed by heating the parts in an unsealed Nabertherm N-150 furnace, thus providing ample oxygen for the combustion and consequently removal of any carbon. The equipment was brought through one cycle of heating to 800°C, with a ramping time of 200 minutes and a hold time of 30 minutes, which was followed by a passive cooling of approximately 12-18 hours. To prevent any delays as a result of this procedure, as it relied on the availability of a suitable furnace, two sets of the alumina parts were provided and used interchangeably throughout the experiments.

Ticks - a distance of 47.5 cm from the center of the crucible to the crucible shaft, and a distance of 51.5 cm from the closed end of the thermocouple sleeve - were drawn using a permanent marker. These ticks would serve as indicators when later positioning small rubber gaskets on the two shafts, something which would later ensure consistent vertical centering within the tube furnace.

To maintain an air-tight seal during experiment, the equipment was fitted with several rubber gaskets. The two largest gaskets, meant to seal the top and bottom end-caps to the inner furnace tube, were cleaned with paper towels.Both top and bottom end-caps were also thoroughly cleaned with paper sheets.

A brass mounting clamp was fastened to the inner furnace tube, making the tube protrude 2 cm above the mounting bracket once lowered into the furnace. After insertion, small amounts of lubricant was applied to the top and bottom end of the alumina tube. One of the large gaskets was lightly lubricated and inserted into a circular groove of the top-cap, which was subsequently lowered into place and gently fixed in place using 4 wing nuts. Taking advantage of some horizontal wiggle room, the top end of the furnace tube was matched up with the rubber gasket of the top-cap, ensuring a snug and symmetric fit.

4.2.2 Sample preparation

Pre-baked pellets were delivered in 5 large production batches (∼130-400 g) and were successively sifted with a 1 mm mesh. During sifting it appeared as if there was a tendency towards large pellets at the top of the batches and smaller pellets at the bottom. As the each batch sifting was done in fractions, scooping or pouring a manageable amount onto the mesh sifter and successively placed in three plastic zip-lock bags, there was a concern that the three bags would have different size distributions. As a result of this, the dosing of pellets for each experimental run was done by sequentially scooping out pellets from the three bags, a procedure assumed to produce a more uniform pellet distribution throughout.

Being somewhat fragile, individual quartz pellets were prone to pulverize when exposed to mechanical impact or compression. Even though the batches were handled with great care, some powder was always present. After weighing and transferring the batches into the crucible, a noticeable amount of powder would stick to the weighing vessel. To avoid having to transfer the fine powder into the crucible, the weight was zeroed out before transferring the sample batch. After transferring the sample, the emptied weighing vessel was brought back onto the scale, and the difference was noted down and would be used as *initial batch weight* in further calculations.

4.2.3 Final assembly

The second large gasket was lubricated and inserted into a circular groove of the bottom end-cap. After inserting the crucible shaft, the end-cap was maneuvered into place and secured to the bottom assembly. The protruding crucible shaft was fitted with a small rubber gasket at the marked tick, raised into the furnace and securely fastened by an adaptor nut. As with the top assembly, gasket and furnace tube was matched up to ensure a event fit, and all wing nuts were tightened.

The thermocouple sleeve was fitted with a rubber gasket and and lowered through the top end-cap and into the furnace. Before reaching the permanent marker tick, extra caution was taken to ensure a good placement, and as soon as the sleeve met resistance - i.e. it had hit the top layer of pellets in the crucible - i was lowered approximately 2 centimeters further, before being secured in place with an adaptor nut.

A final check of all wing nuts and adaptor nuts was made, ensuring a tight and secure fit, before inserting the S-type thermocouple into the thermocouple sleeve. The main gas supply tubing was pushed onto the protruding crucible shaft, making sure there were at least 1 cm overlap, before finally tugging on the tube to verify a snug and secure fit.

4.2.4 Initial gas flushing

After opening the respective valves on the pressurized gas cylinders, the argon purge gas was activated to displace any ambient air contained within the inner furnace tube.

As the equipment had been sitting idle before each experimental run, there were expected to be ambient air present in the main gas supply tubing. Since the main inlet tube received methane and argon from to separate and adjoining tubes, initiating the argon feed would not expel air left in the methane feed tube. The methane feed would be activated at a point where the furnace was hot, and a methane-air mix could result in a partial combustion once entering the furnace and sample batch - potentially altering the surface chemistry of the pellets or posing a health hazard. Based on this, the methane feed was activated for approximately 1 minute in order to flush out any ambient air, an operation that is illustrated in the top left panel in figure 4.2.

Following the short methane flush, a steady flow of 0.5 liter/min of argon was sent through the crucible tube. This inert gas flow had three objectives:

1. It would ensure a positive relative pressure within the inner furnace tube for the duration of the heating procedure, hindering ambient air from entering the equipment. At the same time, it would give the opportunity to verify the integrity of the gas seals during heating, where large fluctuations or large drops of pressure would indicate either breaches or other problems which would be problematic once applying methane.
2. The constant gas flow would also maintain a pellet surface with low partial pressures of atmospheric gases, ensuring the diffusion of air contained within the pourous pellets and subsequent replacement with inert argon gas.
3. To reduce temperature fluctuations when starting the methane treatment. Once initiated, the methane treatment would constitute a mass flow through the heated system, where cold gas both absorbs heat and conceivably changes the transfer of thermal energy. Thus, by providing an alternate gas flow until the methane feed is activated, one would expect less of a temperature response at the start of each treatment.

4.2.5 Coolant check and heat schedule start

To prevent overheating and provide a faster thermal response time, three parts of the lab apparatus was equipped with coolant piping - notably the cylindrical outer steel housing of the furnace, as well as the top and bottom end-caps. Before setting and activating a heating schedule, the supply and return valves of the coolant water system were confirmed set in the open position, implying flow of coolant.

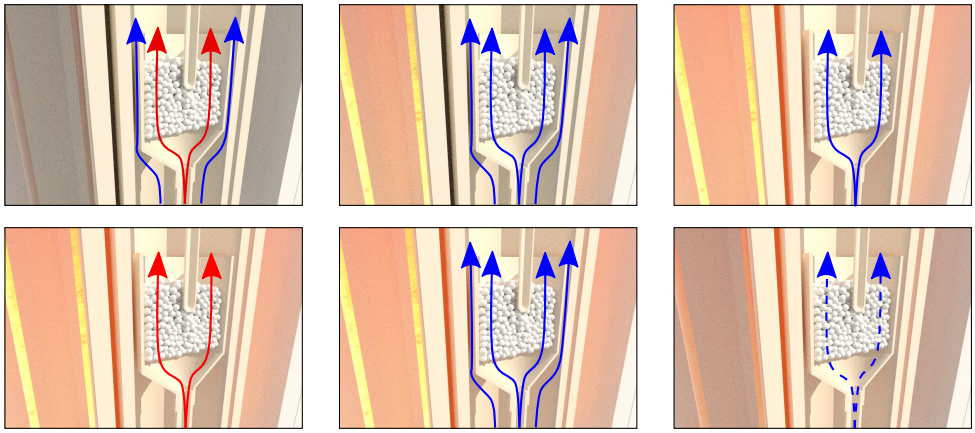

Figure 4.2: At the start of the heat program, argon gas (blue) purge was initiated and methane (red) was flushed through the crucible [top left] for a short time. As heating commenced, methane was switched with argon gas [top center] and after 20 minutes the argon purge was suspended [top right]. The treatment started by turning off argon in the main feed and starting methane feed [bottom left]. At the end of treatment methane was stopped and both argon purge and main feed was opened. After 20 minutes argon purge was stopped, argon in the main feed was adjusted down and the apparatus was left to cool [bottom right].

The main power supply for the furnace was turned on and the TILL-button, which activated the registration of the thermocouples and electric communication between PC and the power supply, was set in active position. The SINTEF NatGas-software was started on the controller PC, which was hooked up to and controlled the furnace power supply. In addition to controlling the power supply, the software monitored both the furnace wall (B-type thermocouple) and crucible thermocouples.

After confirming that both thermocouples were being registered, of which the wall thermocouple was used as feedback for power control, a temperature schedule was set. When at stable high temperatures, the wall thermocouple would read somewhere between 40 to 60°C above that of the crucuble thermocouple - a deviation which would be more pronounced at higher temperatures. Thus the set-point was usually given in the range of 940-950°C and 1050-1060°C for treatments of 900°C and 1000°C respectively.

The heating schedule was started by activating the heating schedule on the PC and subsequently activating the HEAT-button on the furnace power supply.

4.2.6 Purge is suspended

Approximately 20 minutes following the start of the heating schedule, the argon purge gas was turned off, leaving only the steady argon flow through the main gas supply,

as shown in the top right panel of figure 4.2. At the same time, the temperature of the coolant piping was checked by hand to make sure that there was a flow.

4.2.7 Initial temperature stabilization

Approximately 50 to 60 minutes into the heating schedule, the outer wall thermocouple would reach the preset temperature. And as the wall temperature is kept at the set-point, the crucible temperature continues to increase, although at a successively slower and slower rate, finally converging and stabilizing. This behavior can be seen at around 90 minutes in figure 4.3, where the crucible temperature converges towards 885°C while the wall temperature is kept fairly stable at 935°C.

Deviations between actual and desired crucible temperature were corrected for by a corresponding increases of the wall set-point - a procedure which can be seen as a jump in the $T_{\text{set-point}}$ line around 95 minutes in figure 4.3. Further manipulations of the set-point - though less pronounced - can be seen in the remaining interval displayed in the figure. These manipulations were required to achieve the correct temperature, although the ease at which done, as well time used, varied.

The goal of the pre-treatment temperature stabilization was to attain a fairly stable crucible temperature. However, large temperature increases (∼5-10°C) were observed as the methane gas was switched on in the first couple of runs. Accordingly, to prevent the crucible from overshooting the desired temperature, it was usually stabilized at about 5°C below treatment temperature before the methane feed was initiated.

4.2.8 Treatment start

While the treatment start basically consisted of switching from a 0.5 liter/min feed of argon to a 0.5 liter/min feed of methane - illustrated in the bottom left panel of figure 4.2 - the exact procedure was handled with care. As there was a change in the gas supply and flow regulation mechanisms after 11 experimental runs, there were in fact 2 procedures which were applied.

In the first 11 experimental runs, the argon and methane gas flow-rates were each controlled by ALICAT Scientific MC mass flow controllers. Here the exchange between the two flows were made by first setting the argon flow to zero, and quickly and step-wise increasing the flow of methane to 0.5 liter/min in increments of 0.1 liter/min. This was done to ensure that no sudden increase in gas pressure or flow occurred - something that could contribute to sample material or pellets being ejected from the crucible. The procedure took approximately 30 to 60 seconds, after which the exact time was noted down.

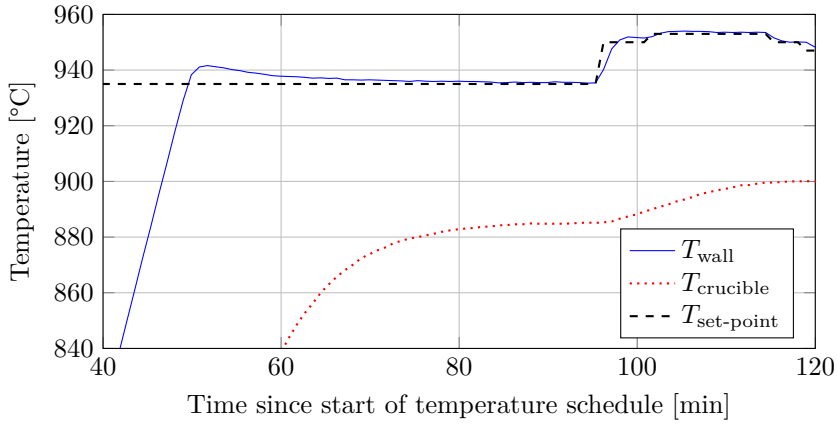

Figure 4.3: Recorded parameters from experimental run # 02 are shown with a resolution of approximately 1 minute. The plot shows how the wall temperature (solid blue) changes in response to the requested wall set-point (dashed). The dotted red line shows how the crucible temperature lags behind and how it stabilizes at approximately 45°C below that of the wall. While no two runs were the same, the general trends of # 02 gives a good representation of the initial heating procedure, with an initial stabilization of crucible temperature followed by corrections of the wall set-point until the desired crucible temperature is reached.

Due to changes in the laboratory infrastructure, the last series of experiments (# 12-# 24) were performed by using a computer controlled Environics Series 4000 gas mixer. A distinct difference between the gas mixer and the ALICAT flow controllers, was the minimum flow requirements of the former. The gas mixer would only start argon gas flow when the set-point exceeded 1 liter/min and methane gas flows exceeding 0.5 liter/min. The flow valve regulation was also considerably slower, having a delay of between 5 to 15 seconds from the gas flow was initiated on the controlling PC until the valve opened. However, the closing of valves was near instantaneous. To accommodate this characteristic of the gas mixer, the treatment consisted of setting the methane gas flow to 0.5 liter/min, entering the number 0 (liter/min) for the argon feed, and waiting until the methane gas flow was initiated before pressing enter. As soon as methane started flowing one could see a pressure increase on the furnace feed line pressure meter, and the enter-tab was pressed on the PC, resulting in an immediate closing of the argon feed.

4.2.9 Treatment temperature stabilization

As mentioned in 4.2.7, one would usually observe a swift crucible temperature increase of about 5-10°C as the methane feed was initiated. Beware of this fact, the crucible had been stabilized slightly below the desired temperature. During the treatment, and particularly in the first 10-20 minutes of each run, the wall set-point was continually adjusted to correct for temperature responses. This correction was done in much

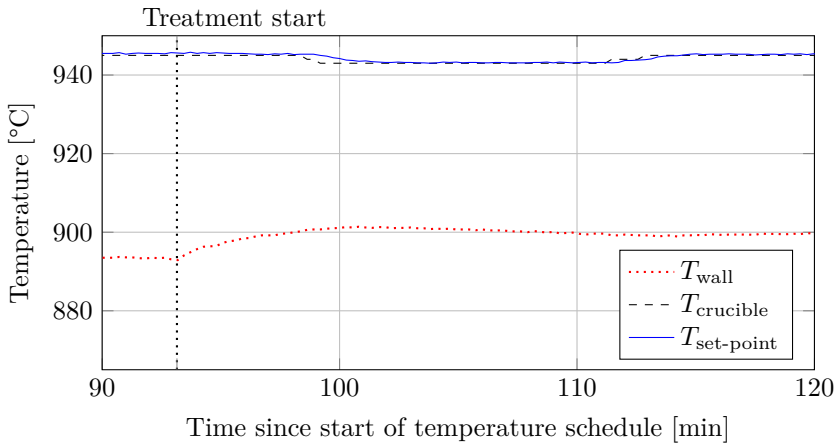

Figure 4.4: Recorded parameters of experimental run #02 are shown with a temporal resolution of approximately 15 seconds. When methane flow was initiated (thick vertical dotted line) there would be an immediate temperature increase in the crucible (dotted red). The wall set-point (dashed black) was adjusted down to reduce the crucible temperature increase. Run # 02 gives a good indication as to how this were done in the rest of the experiments, though temperatures would differ to some extent.

the same way as for the initial temperature stabilization, described in section 4.2.7. An example of this is shown in figure 4.4, where the wall set-point is lowered and subsequently increased to attain the correct crucible temperature.

4.2.10 Treatment stop

At the end of each treatment, the methane feed was switched with argon in the same manner as described for the treatment start in section as described in 4.2.8, the difference being going from a methane feed to the inert argon gas feed. In addition, the argon purge was re-initiated, ensuring the evacuation of all remaining methane from the inner furnace tube, illustrated by the center bottom panel in figure 4.2.

As there were not to be more methane used during the experimental run, the methane pressure control, safety valve and main supply valve were set in closed positions, and the personal gas detector was turned off placed in a charging station.

The final step of the treatment stop consisted of entering a set-point of 0°C into the NatGas-software and turning off the HEAT-button on the furnace power supply, effectively cutting all power to the furnace heating tubes.

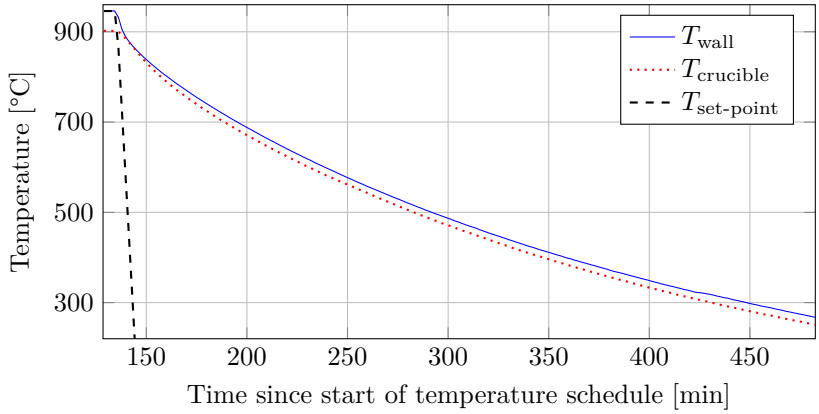

Figure 4.5: Recorded parameters from experimental run # 09 are shown with a resolution of approximately 1 minute and 15 seconds. The plot shows how the wall (solid blue) and crucible (dotted red) typically falls as the set-point is adjusted to 0°C. While factors such as argon flow rate, room temperature and coolant temperature showed some impact on temperatures during cooling, there were no significant differences between the sets. One can also observe a drop from 900°C to 250°C in just under 6 hours (350 minutes), and assuming an exponential temperature decay towards that of the coolant, one could expect to be in the lower range of 100-200°C within 10 hours of treatment stop.

4.2.11 Cooling phase

20 minutes after treatment was stopped, methane would have been sufficiently evacuated from the inner furnace tube and the argon purge gas was turned off as was its corresponding valve on the argon regulator assembly.

Argon flowing through the main supply was adjusted down to 0.2 liter/minute, as illustrated by the bottom right panel of figure 4.2 - a flow rate which would ensure a positive pressure in the furnace as it cooled, avoiding the thermodynamic contraction of cooling gas and a potential backlash of ambient air into the still hot furnace and sample batch. When using the ALICAT controllers, which were not equipped with timing schedule, the gas was let to flow until it was switched off the subsequent day. When using the gas mixer, its argon schedule was set to run for an additional 10 hours post experiment, a period which was assumed large enough to let the samples cool significantly before being terminated - an assumption which seem in accord with the observations made in figure 4.5.

4.2.12 Sample extraction and registration

The samples were meticulously extracted from the inner furnace tube, both to avoid losing any pellet and having carbon fragments deposited on the inner furnace tube dropping into the crucible. Fragments from the furnace tube were very light and

paper-like - with a color and appearance similar to that of pencil graphite - and any flakes which ended in the crucible after extraction were puffed away by blowing gently perpendicular to the crucible top.

When weighing the sample batches, a glass beaker was put on the scale and zeroed out. The beaker was placed upside down atop the crucible, and both were turned gently around and the pellets fell into the beaker. While positioning the beaker on a paper cloth, any stuck pellets were dislodged using tweezers, although care was made to not dislodge carbon deposited directly on the crucible wall. The beaker was weighed and the weight was noted down, along with any comments concerning the run. Finally, the sample batch was transferred to plastic zip-lock bags - which had been marked with chronologiacal numbering, date, temperature and dwell time - and sealed.

4.3 Choice of experimental setup

As this thesis originated from the larger efforts being undertaken in the SINTEF-led SiNG-project, there was already some knowledge and experiences to expand upon. Most notably, an experimental setup had already been used in a handful of experiments during the first half of 2014. These previous experiments had the same objectives as this work, to treat samples with gas at given temperatures and dwell times and observe weight increase.

Even though there existed a viable experimental setup, other possible ways of performing the experiments were given consideration. While the primary objective of the experiments was to observe the amount of carbon deposited under different conditions, the primary objectives of the experimental setup (or *apparatus*) was to:

1. Achieve and maintain a stable temperature
2. Treat samples with gas

The apparatus which had been used in the previous SiNG-runs, conformed to both experimental setup objectives. However, achieving the main objective of the experiments - to measure weight increase as a function of time - was not an integral part of the system. This meant that individual test runs had to be undertaken at discrete time intervals, and at the completion of each individual run, the samples had to be extracted and weighed. As the apparatus in question (described in depth in section 4.4.2) required considerable time for preparation and temperature increase, as well as a substantial cool off period post experiment, one were only able to conduct one experimental run per day.

Apart from being decidedly time-consuming, the SiNG apparatus had some advan-

tages. It was able to handle sample batches of approximately 50 cm^2, had a high heat capacity (providing stable temperatures) and a low threshold for use. In addition, each treated batch would have a carbon deposit which should represent a snapshot of the growing carbon layers at a specific temperature and dwell time, given there were no structural changes during the cooling or subsequent exposure to atmospheric oxygen.

In an ideal experimental setup, one would be able monitor weight increase, gas composition and surface structure *in situ*. While different surface characterization techniques may be difficult to implement at experimental conditions, there does in fact exist equipment which combines both the main experimental and the apparatus objectives. An example of such a unit is the *Tapered Element Oscillating Microbalance* (TEOM), which not only controls temperature and gas exposure, but continually monitors weight change during treatment. Although there certainly existed scientific equipment which could provide an alternative to the SiNG-apparatus, no such units were currently available at neither NTNU's nor SINTEF's facilities.

4.4 Samples and gas treatment

From the outset, the main components of interest for this work were decidedly quartz and natural gas. Both *quartz* and *natural gas* are somewhat generic terms, as they apply to a range of compositions and purities.

Sample material

Quartz may apply to a wide variety of crystalline minerals composed of mainly SiO_2. When deciding on the specific silica based material to use in this work, two main routes seemed most interesting. One possibility would be to choose an extremely high purity homogenous α-quartz - a choice which would limit any secondary and unwanted reactions to an absolute minimum. A highly uniform sample material would also narrow the scope with respect to differences in gas and material interaction for different crystal surfaces. The second possibility would be to choose a pre-reduction industrial grade sample. Such a sample would be more relevant to real-world applications, where silica feed material for carbothermal reduction often contains up to 0.5 % impurities.

The final choice of sample material came down to two factors, availability and applicability. As this thesis work was associated with the SiNG-research project, Elkem Solar were happy to provide substantial batches of cleaned quartz raw material suited for carbothermic reduction. More importantly, by choosing the material provided by Elkem Solar, one would get indications of the ease at which carbon could be deposited in an actual industrial process.

Sample shape

Prior to the original SiNG-experiments, SINTEF recieved a batch of pre-crushed coarse quartz particles from Elkem. A portion of this batch was extracted and went to further crushing to a particle diameter[1] of $d_{50\%} = 25\ \mu m$ and sintering into spherical pellets in the range of 1-3 mm. Makeshift tests were performed by *Pål Tetlie* and *Ingeborg Solheim* (both SINTEF employees) to decide on appropriate gas flow-rates. Both coarse particles and pellets were placed in the experimental crucible and exposed to ascending gas. Based on these initial tests, it was concluded that both pellets and particles remained securely in the crucible at gas flow-rates below 1.5 liter per minute, and a final *safe* flow-rate of 0.5 liter per minute was decided upon.

A main observation in the preceding SiNG-experiments was a strong correlation between sample shape and carbon deposits - or more precicely - exposed to the same conditions, sintered quartz pellets gained substantially more carbon than coarse quartz particles. While not conclusively, this was attributed to different surface-to-weight ratios of the respective sample types. Based on an assumption that the deposition would be highly reliant on the quartz surface area exposed to gas, it was decided to focus on the larger-surface sintered quartz pellets.

4.4.1 Treatment temperature and duration

The previous trial runs performed by the SINTEF team had given some indications as to which temperature level one could expect to see noticeable amounts of carbon deposition. Based on this, an initial series of runs at 700°C, 800°C and 900°C were agreed upon. Since the SiNG experiments had a duration of 320 minutes, it was decided to apply the same treatment duration for the initial runs, giving the possibility of comparing the data.

After concluding four initial runs, it was observed that there were very little carbon deposited on samples treated at 700°C and 800°C. As there were already one result at 160 minutes for the 900°C(run # 03), a run that showed nearly as much deposited carbon as the sample that had been treated at 320 minutes, and given that the low temperature samples did not show any significant deposits, it was decided to do two complementary runs as well as two runs at 1000°C.

On concluding 8 runs, both having corroborated the initial observation for run # 03 and gained consistent results for 1000°C, a plan for the remaining experimental runs were made. This consisted of sets of two runs for each temperature level for the durations 20, 40 and 80 minutes, as well as run at 320 minutes for the 1000°C.

[1] The designation $d_{50\%}$ (*also* d_{50} or d50) represents the mass-median-diameter (MMD), which is the median particle diameter based on particle mass.

As the planned experiments were finished, already having observed some trends in the data, an additional run at 320 minutes at 900°C were decided upon. While a treatment were performed, it did not proceed ideally as there were experienced gas pressure buildup in the furnace and leading to some pauses in the treatment. A last attempt experienced the same problems, resulting in an aborted treatment after 210 minutes.

4.4.2 Principal layout

While the overall purpose of the experimental setup can be summed up as *exposing quartz to methane for a certain time and at a specific temperature*, there was a substantially larger set of individual requirements which had to be met. Not only were samples to be treated, but this should be done in a scientifically robust and consistent manner while maintaining a high level of safety. The handling of combustible gases in particular, such as methane, requires a strict set of precautions - mainly attributed to avoiding leaks, handling off-gas and in the case of any leaks, gas detection. However, while safety must be the main priority, a lot of the measures ensuring safety in the laboratory environment also contribute to more rigorous scientific findings.

Integrity of gas carrying equipment

With respect to both experiment and safety, the integrity of the gas carrying equipment was paramount. Leakage of methane would obviously pose a hazard in the laboratory, but inclusion of ambient air or other gases would be equally detrimental in an experimental aspect. The presence of oxygen inside a heated chamber carrying methane could not only lead to explosions, it would also introduce secondary reactions and possibly compromise the results. Even after treatment, at a time when methane has been evacuated from the still-hot apparatus and replaced by inert gas, any oxygen present would react with and remove deposited carbon. To lower the risk of deposited carbon reacting with air, the treated batch were to be kept in an inert atmosphere until the apparatus and samples had reached room-temperature. All these considerations accentuated the importance of having a hermetically sealed system, where you had full control over the atmospheric conditions of the samples during elevated temperatures.

Gas treatment and temperature control

Three factors which carry less of a safety concern, but are of high scientific importance, are gas compositions, gas application control and temperature control. With respect to the gases applied, both the inert argon and the methane gases were of high purities (CH_4 5.5 and Ar 6.0). Being able to accurately maintain the temperature at a certain level, ensures consistency between individual runs as well as the accuracy of any relationships derived from the experiments - i.e. one would expect a greater variation

of deposited carbon mass in two similar runs, when the treatment temperature fluctuates between +/- 10°C as compared to a fluctuation of +/- 1°C. Different factors which would influence the temperature of the sample batch, and the fluctuations thereof, were:

1. Temperature of the gas
2. Heat capacity of the gas
3. Heat conductivity of the gas
4. Chemical reactions:
    a) Between samples and the gas
    b) Within the gas

In all respects, the two gases were of such a purity that they should be well represented by any calculations based on the properties of pure substances. As the experimental procedure called for a switch from inert gas to methane at elevated temperatures, temperatures might fluctuate as a result of this. Disregarding any chemical reactions, the main factors contributing to a change of the temperature in the sample batch would be the temperature, as well as the heat capacity and conductivity, of the passing gas.

The gases were supplied by room tempered pressurized gas canisters/cylinders, where one would expect a drop in gas temperature upon the release and subsequent decompression of the gas. The gases were led through both and rubber tubing at a length of approximately 4 meters before entering the experimental apparatus. Before reaching the crucible containing the sample batch, the gas had to travel through a ∼60 cm long hollow alumina shaft, of which 40 cm were enclosed within the vertical tube furnace. The gas flowing through the batch would have a temperature which depended on its temperature upon decompression, as well as heat absorbed both through the external supply tubing and the internal crucible shaft.

Moreover, as the thermal energy to the crucible itself would be supplied radially by both conductive and radiative heat transfer, the heat conductivity of the gas would be of importance.

4.5 Scanning Electron Microscopy (SEM)

The main result from the experimental treatments would be provided as weight increases. While this was the most important topic of this study, some thought were given to possible alternative analysis that could add to our knowledge of the processes taking place. In this respect SEM was a natural choice, being able to provide detailed images of the treated samples' micro-structure.

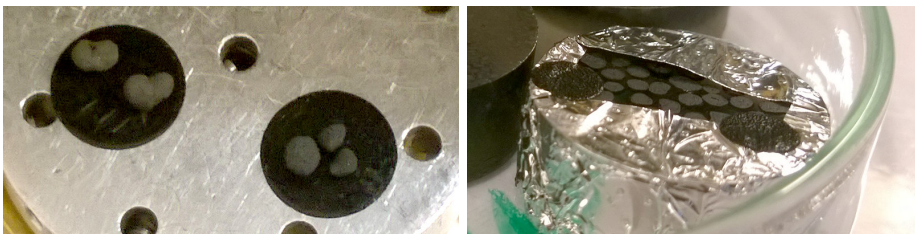

(a) (b)

Figure 4.6: Regular treated sample pellets on the SEM mount (a) and resin-embedded samples wrapped in aluminium foil for the assessment of internal structure (b).

It is assumed that that the would have a general knowledge of SEM, this will not be given an extensive review in this section. For those wanting to delve into the subject, the book *Physical Principles of Electron Microscopy*[19] can be recommended.

Since the main focus was the micro-structure of the sample surfaces, the majority of the images were captured using the SEM secondary *or in-lens* electron detector. This enabled the opportunity for better resolutions at high magnifications. As the voltage applied in the SEM controls the penetration depth of electrons on the sample surface, voltages of <7 kV were used.

Both single pellets and resin-embedded (EPOXY) samples were analyzed. The resin embedded samples had been ground down to uncover the cross section of treated pellets, giving a view of the internal structures of the pellets. While single pellets were placed directly on conducting carbon tape and analyzed, the embedded samples had to be coated with carbon to provide conduction and stop the buildup of charge on the surface as well as wrapped on aluminium foil when placed on SEM mount. Examples of the samples are shown in figure 4.6

4.6 Surface measurements - BET

Samples were sent to surface analysis by the Brunauer–Emmett–Teller (BET) method[20]. Here samples are exposed to varying pressures of non-reactive gases. As the pressures increase gas molecules start to deposit on the sample surface. As the gas condenses on the surface sample, the pressure falls. By measuring this pressure response, one can assess the exposed surface area of the sample.

Based on availability, only a total of 11 samples were sent to analysis.

Chapter 5
Observations & Results

For the analysis of high temperature carbon deposition on quartz from methane gas, there were three main observational parameters or results:

1. **Mass deposition data**
   Initial and final sample weights were registered for all samples, together with their respective experimental parameters (Run #, temperature, dwell time and comments). A temperature history of each individual run was also logged.
2. **Specific surface area**
   A selection of 11 treated samples, as well as the 5 untreated pellet production batches, were sent to BET-analysis[1] to attain specific surface areas.
3. **Scanning Electron Microscopy (SEM)**
   Before starting the experiments for this research, samples from previous experiments made in the SiNG project(as mentioned in section 4.3) were viewed by SEM. Of the experiments conducted in this research, 6 runs had their exterior pellet surfaces observed by SEM. Three of the runs were also embedded in epoxy and ground down until they showed a cross section of the pellets.

5.1 Mass deposition data

A sum total of 24 experimental runs were performed, of which 10 were conducted at 1000°C, 12 at 900°C, 1 at 800°C and 1 at 700°C, as seen in table 5.1. In addition to the weight data, temperature logs showing the the thermal history during the experiments were recorded, and are briefly mentioned in section 5.1.2.

The majority of the experiments were performed at specific intervals of 20, 40, 80, 160 and 320 minutes (geometric progression of $20 \cdot 2^n$ minutes), although two runs

[1] Brunauer–Emmett–Teller (BET) analysis consists of exposing a sample to an inert atmosphere while increasing the pressure. By recording pressure responses to applied gaseous pressures, one is able to calculate the effective surface area of the sample.

deviated from this practice, namely runs # 08 and # 24. The former being the result of an erroneous calculation, while the latter followed a blockage of the furnace off-gas system. Moreover, runs # 23 and #24 both experienced blockage in the furnace off-gas, however, # 24 was the only occurrence where further methane treatment was aborted and the experiment stopped.

With the exception of experimental runs # 23 and #24, all runs were performed as a continuous operation with no pauses.

For the treatments at 1000°C, and especially that of 320 minutes (# 14), groups of individual pellets had been aggregated or fused together in larger lumps.

Experimental run # 01 was performed at 700°C and showed no discoloration when visually inspected. A subsequent weighing of the sample showed a loss of 0.0266 g or 0.07 % of sample mass.

Experimental run # 04 was performed at 800°C and showed a slight greyish discoloration, indicating a very fine layer of deposited carbon and a slight weight increase of 0.0125 g or 0.07 %.

5.1.1 Weight increase data

All experimental runs at 900°C and 1000°C are displayed in figure 5.1, where percentage weight increase is plotted relative to the methane exposure time. The 5 production batches from which the pellets originated is indicated with different symbols, and the marks are color coded to separate the two temperature series.

Table 5.1: Weight increase data. The data is displayed chronologically, where the rightmost column represent the percentage of weight increase for each experimental run. Pellet production batch number - out of 5 batches used throughout the experiments - are displayed in the first column. Irregular runs and observations are indicated with symbols in the second column and commented below the table.

Batch no.	Experimental			Weight			
	Run no.	Temp.	Dwell	Initial	Final	Difference	
		[°C]	[min]	[g]	[g]	[g]	[%]
1	# 01	700	320	40.1761	40.1495	-0.0266	-0.07
	# 02	900	320	40.6487	41.2714	0.6227	1.53
	# 03	900	160	40.0262	40.5325	0.5063	1.26
	# 04	800	160	40.0115	40.0240	0.0125	0.03
	# 05	1000	160	40.1222	44.5668	4.4446	11.08
	# 06	900	160	40.0084	40.6161	0.6077	1.52
	# 07	1000	160	40.0408	44.7653	4.7245	11.80
	# 08$^{\diamond}$	900	130	40.0284	40.4935	0.4651	1.16
2	# 09	900	20	40.0200	40.0495	0.0295	0.07
	# 10	1000	20	40.1669	40.6399	0.4730	1.18
	# 11	1000	20	40.0393	40.5916	0.5523	1.38
	# 12	900	80	40.0780	40.2410	0.1630	0.41
	# 13	900	40	40.0709	40.1558	0.0849	0.21
	# 14	1000	320	40.8057	48.8329	8.0272	19.67
3	# 15	900	40	40.0894	40.2754	0.1860	0.46
	# 16	1000	40	40.0894	41.4044	1.3150	3.28
4	# 17	1000	40	40.2220	41.4437	1.2217	3.04
	# 18	900	80	40.3219	40.6152	0.2933	0.73
	# 19	1000	80	39.9630	42.2337	2.2707	5.68
	# 20	900	20	40.1075	40.1464	0.0389	0.10
	# 21	1000	80	40.0650	42.1675	2.1025	5.25
	# 22	1000	80	40.5561	42.9811	2.4250	5.98
	# 23*	900	320	41.4688	43.4412	1.9724	4.76
5	# 24*	900	210	40.1826	40.9156	0.7330	1.82

$^{\diamond}$ Erroneously ending run too early. Lost two pellts when extracting from furnace.

* Intermittent periods of argon owing to pressure buildup - i.e. discontinous treatment.

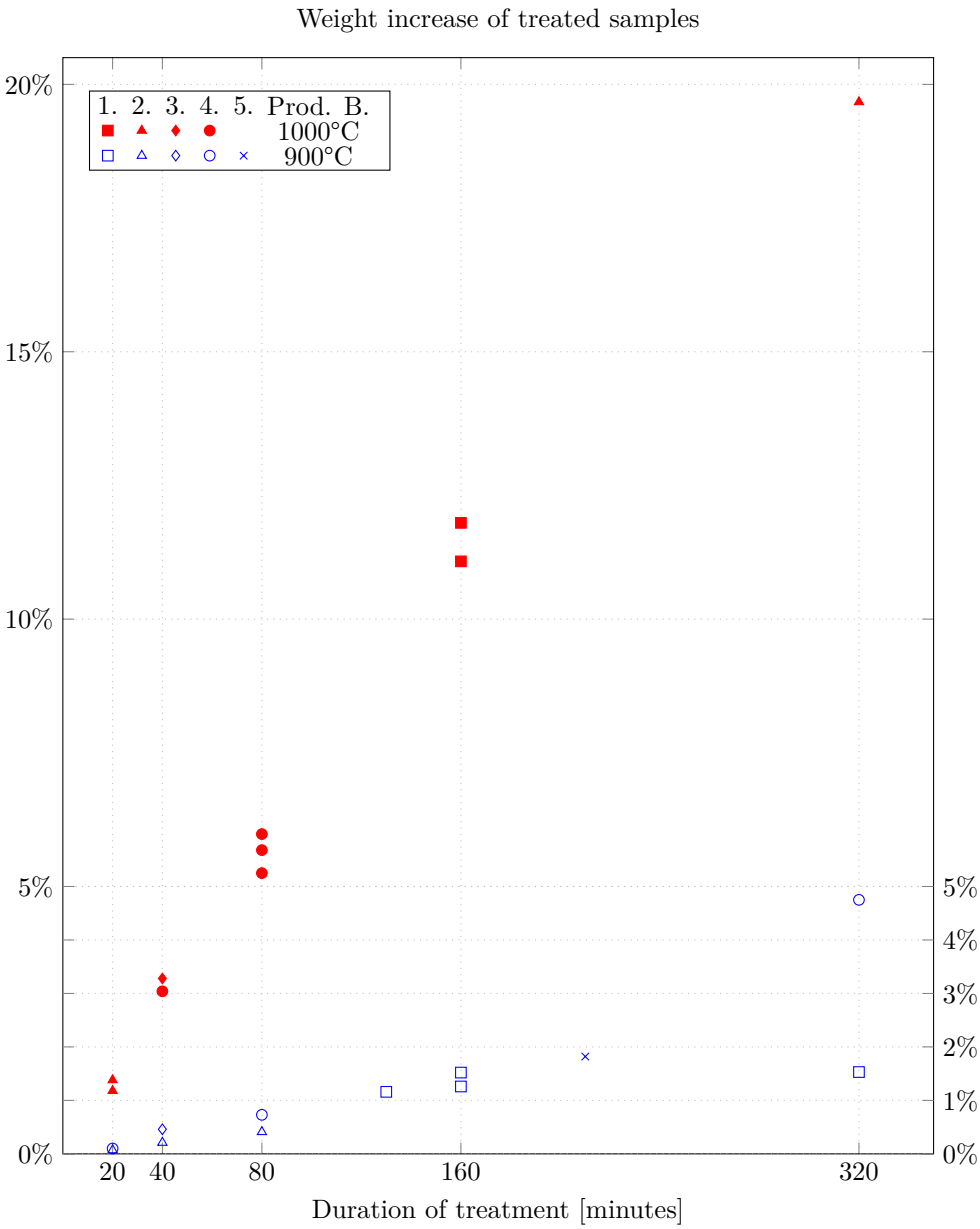

Figure 5.1: Percentage weight increase for samples treated at 900°C (**blue**) and 1000°C (**red** with fill). Different symbols indicate the pellet production batch (as indicated with 1.-5.) of the specific runs. Runs at 1000°C shows a consistently higher weight increase than those at 900°C. Sample batches treated at 1000°C for 20 minutes showed approximately the same weight increase as sample batches treated at 900°C for 160 minutes.

5.1.2 Temperature logs

At the end of each experiment, as one closed the SINTEF NatGas software, a temperature log would be sent automatically by e-mail. There were instances when these logs were not delivered correctly, but 20 out of the 24 were recieved, of which 18 were from the 900°C and 1000°C runs. These logs have been summed up in 18 histograms and displayed in figures 5.2 and 5.3.

5.2 Specific surface area

Since there already was suspicion that surface area would be an important factor in the rate of deposition, samples were sent to BET analysis. At the time, the availability of qualified personnel which could conduct the analysis dictated that only a selection of the samples could be analyzed. To be able to carry out manipulations of the data and conduct further analysis, it was important to know the surface areas of all the 5 production batches, so these were given priority.

In addition to the production batches, samples were selected from the experimental runs at 900°C and 1000°C. These samples represented the experimental runs which had gained the least and most weight at 20 and 320 minutes, in addition to a sample at 160 minutes from the 900°C which had a comparable weight increase to that of the 1000°C sample that had been treated for 20 minutes. In addition 6 more samples were selected on the basis of having a fair distribution among weight increases and treatment durations. All in all, 7 samples from the 900°C run was analyzed and 4 from the 1000°C.The results of the BET surface analysis is presented along other relevant factors in table 5.2.

5.3 Scanning Electron Microscopy

In total, 6 different samples from the experiments were observed with SEM.

2 samples from earlier experiments, carried out in the SiNG project, were also analyzed with SEM. Table 5.3.

5.3.1 Exterior surfaces

A large set of exterior surface images were captured at different magnifications, as illustrated by the images in figure 5.4. As can be expected, samples showing larger weigh increase also showed a thicker layer of carbon. While samples with low weight increase showed a more structure, as only a thin layer covered the quartz particles, the samples with large weight increase showed a more even surface.

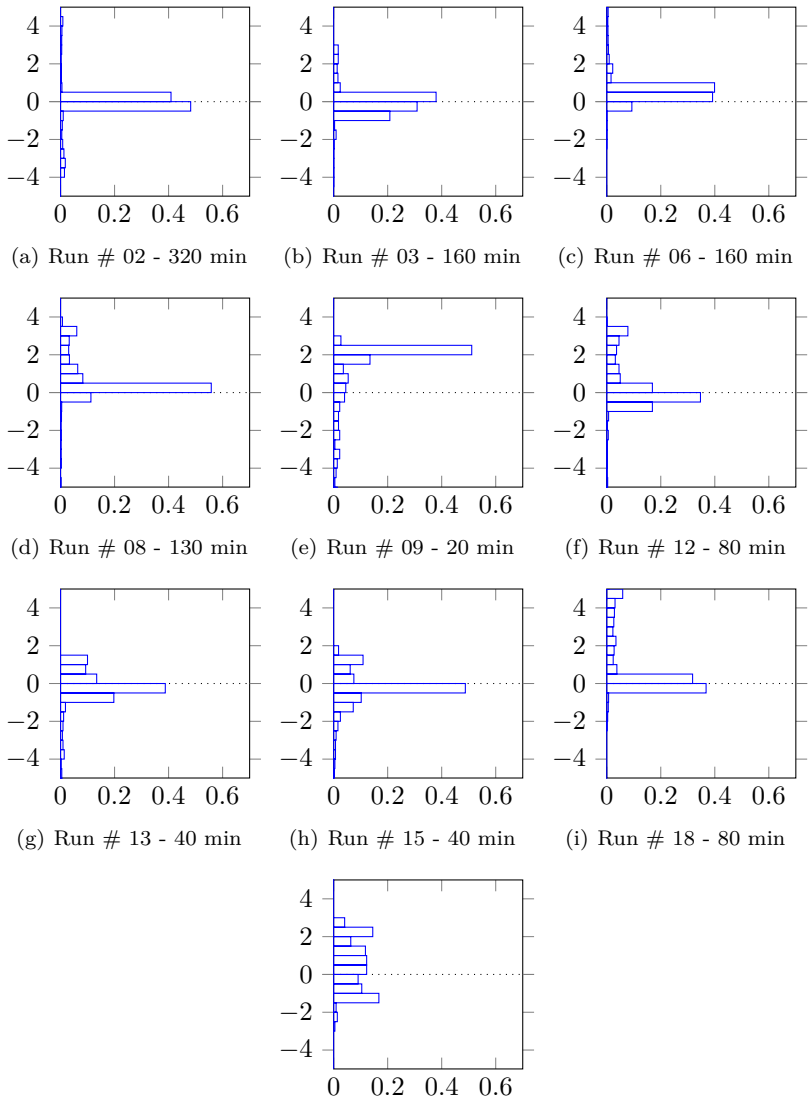

(a) Run # 02 - 320 min (b) Run # 03 - 160 min (c) Run # 06 - 160 min

(d) Run # 08 - 130 min (e) Run # 09 - 20 min (f) Run # 12 - 80 min

(g) Run # 13 - 40 min (h) Run # 15 - 40 min (i) Run # 18 - 80 min

(j) Run # 20 - 20 min

Figure 5.2: The above figures (a - j) show histograms from the available temperature logs at 900°C (runs # 23 & # 24 were not available), where the vertical axis represents intervals from 5 degrees °C below to 5 degrees °C above 900°C and the horizontal axis tells which time fractions (out of 1) have been spent on the different intervals. Overall, the recorded temperatures show only small deviations from the desired temperature, with the longest runs (a - d) having the smallest deviations and the shortest runs (e - j) having the largest.

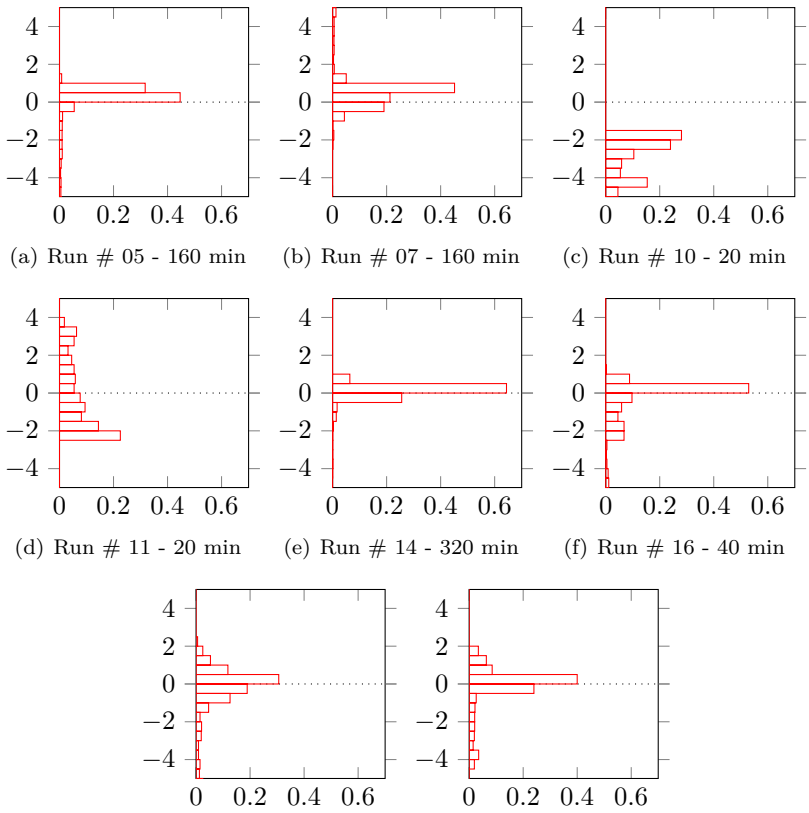

(a) Run # 05 - 160 min (b) Run # 07 - 160 min (c) Run # 10 - 20 min

(d) Run # 11 - 20 min (e) Run # 14 - 320 min (f) Run # 16 - 40 min

(g) Run # 19 - 80 min (h) Run # 21 - 80 min

Figure 5.3: The above figures (a - h) show histograms from the available temperature logs at 1000°C (except runs # 17 and # 22), where the vertical axis represents intervals from 5 degrees °C below to 5 degrees °C above 1000°C and the horizontal axis tells which time fractions (out of 1) have been spent on the different intervals. Overall, the recorded temperatures show only small deviations from the desired temperature, with the longest runs (a - b, e - h) having the smallest deviations and 20 minute runs (c - d) having the largest.

Table 5.2: Surface analysis data are shown in the rightmost three columns, most notably the specific surface area (m^2/g). Both untreated and treated samples were analyzed, of which all treated samples show a larger surface area than the untreated ones.

Production batch	Experimental				Surface analysis data		
	Run no.	Temp [°C]	Dwell [min]	Weight gain	Weight [g]	Area [m^2]	Specific surface [m^2/g]
Untreated quartz pellets							
no. 1					1.6551	0.53	0.320
no. 2					1.9068	0.46	0.241
no. 3					1.2793	0.43	0.336
no. 4					1.2996	0.52	0.400
no. 5					1.556	0.50	0.321
Treated quartz pellets							
no. 1	# 02	900	320	1.53 %	2.0074	1.77	0.882
no. 1	# 03	900	160	1.26 %	2.4347	2.15	0.883
no. 2	# 09	900	20	0.07 %	2.4543	1.02	0.416
no. 2	# 12	900	80	0.41 %	1.9494	1.00	0.580
no. 3	# 15	900	40	0.46 %	1.4722	1.03	0.700
no. 4	# 20	900	320	0.10 %	0.6513	0.29	0.445
no. 4	# 23	900	20	4.76 %	0.7435	0.84	1.130
no. 2	# 11	1000	20	1.38 %	2.3237	2.14	0.921
no. 2	# 14	1000	320	19.67 %	2.2366	1.76	0.787
no. 4	# 17	1000	40	3.04 %	1.1630	1.32	1.126
no. 4	# 19	1000	80	5.68 %	1.5838	1.80	1.137

Table 5.3: Summary of which samples were observed with SEM and the type of observation. Samples marked *Exterior* (•) had images captured of their outer surface while samples marked *Interior* (⋆) have been embedded in EPOXY and had their internal surfaces and passageways reviewed.

Run no.	Temperature	Interior	Exterior	Treatment time	Weight increase
# 04	800 °C		•	160 min	0.03 %
# 03	900 °C	⋆	•	160 min	1.26 %
# 09	900 °C		•	20 min	0.07 %
# 07	1000 °C		•	160 min	11.8 %
# 11	1000 °C	⋆	•	20 min	1.38 %
# 14	1000 °C	⋆	•	320 min	19.67 %

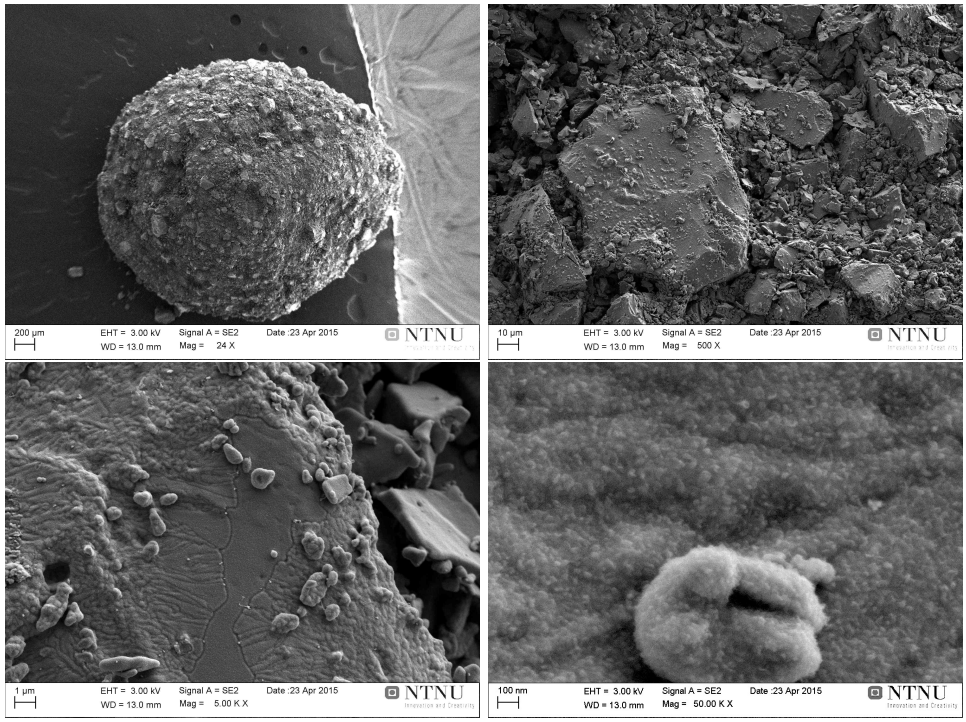

Figure 5.4: Scale width These exterior surface SEM-images of run # 03 shows the shape of an individual pellet [top left] as well as zooms of roughly 1:20 [top right], 1:200 [bottom left] and 1:1000 [bottom left]. As seen in the top panel, the shape is fairly spherical with a diameter of approximately 2 mm. One should be aware that distortions as a result of the intrinsic properties of the SEM apparatus may appear in top left image.

When comparing two samples at different treatment temperature but the same weight increase, there were no remarkable differences.

5.3.2 Interior surfaces

Samples from runs # 03, # 11 and # 14 were embedded in epoxy and observed in the same manner as the exterior SEM captures. An illustration of the images captured can be viewed in figure 5.5.

When viewing the interior of samples with the same weight increase but different treatment temperature, one could not see any apparent differences.

One important observation was that the interior of the samples appeared to show more structure than their outer surface, of which SEM images had been captured earlier. This indicated that there was less deposition on the interior structures of the samples.

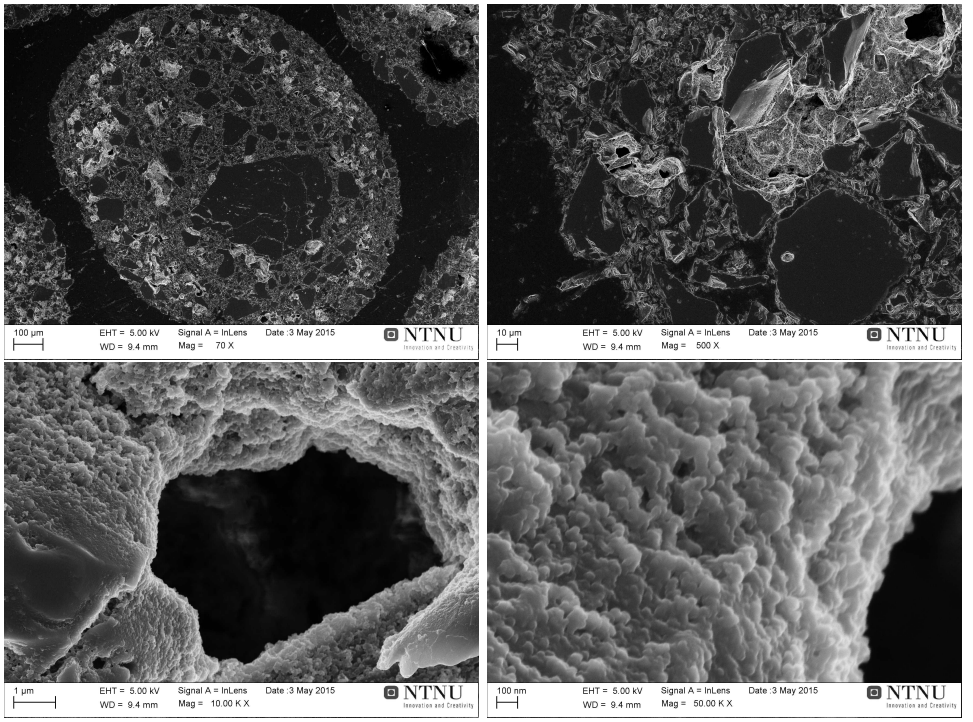

Figure 5.5: These SEM-images from an EPOXY-embedded sample (run # 03) shows the cross section of an individual pellet [top left] as well as zoom of roughly 1:10 [top right], 1:100 [bottom left] and 1:1000 [bottom right]. The cross section in the top left panel shows a fairly circular shape, with the longest and shortest cross sectional diameters being approximately 1.4 and 0.9 mm respectively. Apparent in the zoomed images are the abundance of inter-particle spaces and passageways.

Chapter 6
Analysis & Discussion

The main observations were differing weight increase rates at the different temperature levels, increase in surface area as carbon got deposited and the presence of deposited carbon on the particles interor surfaces.

6.1 Main observations

6.1.1 Weigh increase data

The most striking feature of the plotted data, is the difference in deposition rates between samples treated at 900°C and 1000°C. The earlier displayed figure 5.1 has been reproduced in figure 6.2 and, assuming linear weight increases with time, fitted with trend lines intercepting the origin. The trend lines, which have coefficients of determination of $R^2_{1000°C}$= 0.98 and $R^2_{900°C}$= 0.69, show a 7 times higher rate of deposition for 1000°C compared to 900°C.

6.1.2 Specific surface data

A second compelling observation, is that of the treated sample surface data as seen in table 5.2. Two of the samples treated at 1000°C exhibit specific surface area increases of 290 % compared to the initial quartz pellets (# 11 & # 14), despite having been exposed to methane for vastly different periods as well as having substantially different weight gain. Similar observations, although at a lesser extent, holds for the samples treated at 900°C.

6.1.3 Internally deposited carbon

Pellets from runs # 03 (160 minutes, 900°C) and # 11 (20 minutes, 1000°C) were given an examination of both externally and internally deposited carbon by SEM. These samples had shown approximately the same weight increases and were expected to show different surface characteristics in the case of different underlying deposition

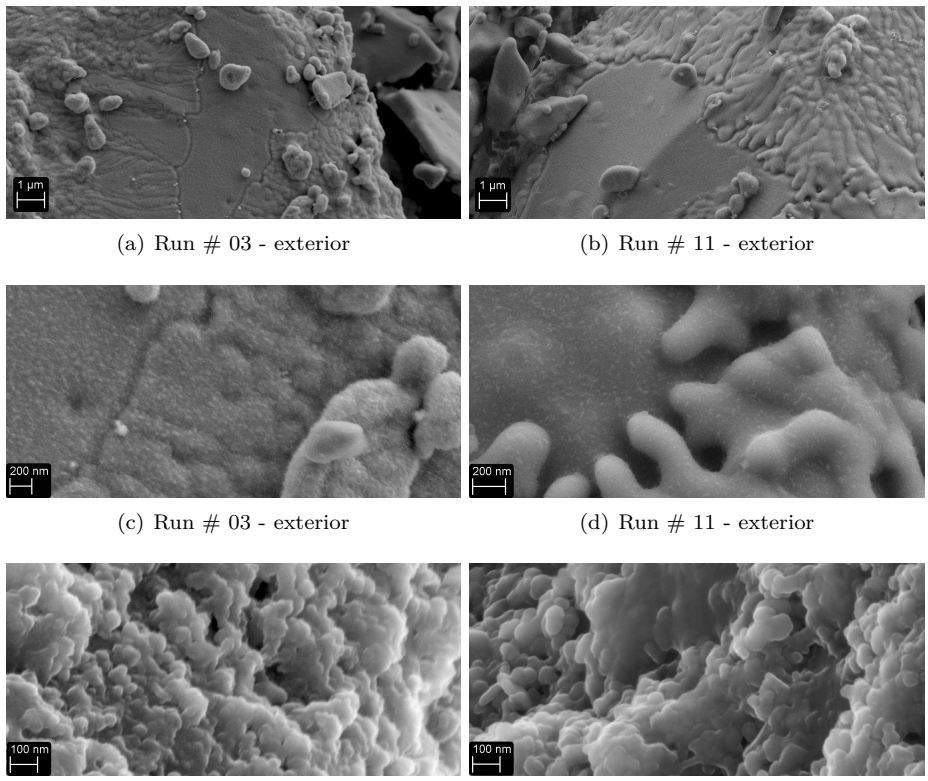

(a) Run # 03 - exterior

(b) Run # 11 - exterior

(c) Run # 03 - exterior

(d) Run # 11 - exterior

(e) Run # 03 - interior

(f) Run # 11 - exterior

Figure 6.1: Exterior (a - d) and interior (e - f) SEM images of pellets from samples # 03 and # 11, which were treated at 900°C for 160 minutes and 1000°C for 20 minutes respectively. The images which are side by side are of the roughly same scale, where the left images represent run # 03 and the right images run # 11. There aret no striking differences between the image from the two temperature levels. There seem to be a difference between the exterior and interior images, where the interior images show more massive structures while the exterior surfaces have a smoother surface, something which could indicate that the interior structures have a thinner carbon layer. However, one should note that images (c) & (d) are at twice the scale of images (e) & (f), and that the former is taken by the primary electron detector while the latter with the second electron detector, both having an impact on how the images appear.

mechanisms. Both the exterior and interior surfaces seemed to be relatively similar for the two temperature levels, as is briefly discussed below figure 6.1. There appeared to be a difference between the interor and exterior images, but no definate conclusion could be drawn.

6.1.4 Observed inconsistencies in procedure

As to the quality of the data, there are particularly two subjects that should be addressed, the two runs with pauses in treatment (# 23 & # 24) as well as the loss of pellets in experimental run # 08.

Compared to the two experimental runs of 160 minutes at 900°C (runs # 03 & # 06), which are closest to run # 08, showed a slightly higher weight increase - however, out of a sample batch with 40 g of pourous pellets, two solid spheres of quartz, each with a diameter of 3 mm (in the upper range of our samples), would constitute a weight of only 0.075 g or 0.19 %[1] of our initial weight. In addition to this, run # 08 was of 30 minutes shorter exposure and lines up nicely with the overall data at 900°C, as can be seen in figure 6.2. Based on this, it can be assumed that the loss of two pellets in run # 08 had no significant impact on our data.

The two treatments that were paused as a result of pressure build, having intermittent periods of argon instead of methane, could give a greater cause for concern. Sample # 24 was initially exposed to methane for approximately 190 minutes, and after a 20 minute pause in the treatment, resumed. In the last period of treatment, it was exposed to varying flow rates of methane, until the treatment was aborted after a total of 210 minutes. Sample # 23, on the other hand, had several intermittent periods of argon gas flow, and the experiment ended after completing the total of 320 minutes exposed to the methane gas. Both the pauses in the methane treatment and the short periods of pressure buildup could affect the the final results. One should also notice that of the two 1000°C runs at 320 minutes, sample # 23 showed a three times higher weight increase.

An additional matter of interest, would be the consistency of the individual treatments. Logs from the crucible thermocouple, as presented in figures 5.2 and 5.3, showed some slight deviations from the desired treatment temperatures for individual runs. The fraction of time spent close to the desired temperature was larger - as one might expect as a result from the initial temperature stabilization - for the longer runs.

All in all, the most obvious errors in the experiments, with the exception of run # 23, should not be expected to play a major role. However, as quality and consistency of the individual runs are of great importance, a broader list of possible error sources will be discussed in section 6.5.

[1] Based on the assumption of solid spherical quartz at a density of 2.65 g/cm^3 and radius of 3 mm.

6.1.5 Possible controlling factors

Right at the outset, it could be beneficial to identify different factors expected to influence the rate of deposition and do some rough initial comparisons to the data:

- **Temperature** would be expected correspond positively with the deposition rate, where at higher temperatures, one would see higher rates of deposition. This is well in accordance with our observations, where the samples amassed approximately 7 times more carbon at 1000°C than at 900°C.
- **Surface area** should be expected to correspond linearly to with deposited mass, where higher surface area would provide a greater interface for methane to interact - at least at temperatures where the gas is not likely to interact mainly with itself. While it is hard to ascertain how large a factor this was by looking at figure 6.2, the overall consistency of the two temperature series indicate that, by assuming a constant surface to weight ratio and using weight as a proxy, the initial surface area corresponded well to deposited carbon. By further looking at the specific surface data (5.2) there is a hint at a relatively stable surface area, although at a different level than at the outset.
- **Surface reactivity** or how likely the methane is to react with a specific surface, is less likely to be identified in figure 6.2. One might speculate in different reactivities of quartz and carbon surfaces, moreover, one could further theorize that the surface changes reactivity as layers of carbon are added to the surface.
- **Particle geometry** would be expected to come into play when the deposited carbon layer thickness starts to influence the overall particle surface - i.e. as the surface of an expanding sphere increase with its diameter. The shrinking diameter of micro-pores inside the pellets as well growing and coalescing particle surfaces would also be examples of such an instance.
- **Surface topography** would correlate to particle surface, whereas increased surface structure or roughness would contribute to an increase of surface area, the opposite would be the case if deposited carbon evens out the surface.

To summarize, the factors considered as important mechanisms were all related to temperature, surface area and the methane reactivity of the surface. These matters will be given further consideration in the following sections, as we try to understand what really happened on the sample surfaces during deposition.

6.1.6 Homogenization of observations

One caveat concerning figure 6.2, is that it relates weight increase to initial weight. While one could expect a link between the two, it should only be with weight as a

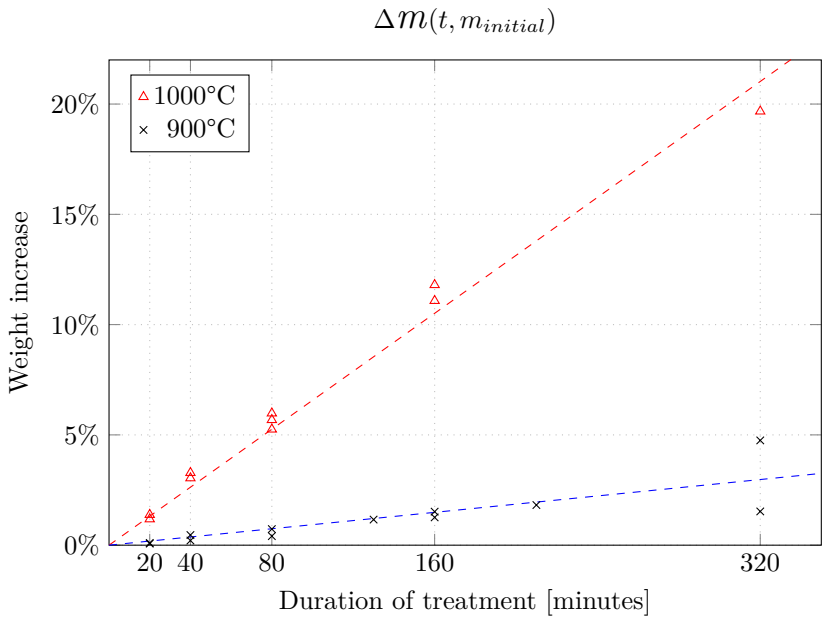

Figure 6.2: Percentage weight increase for samples treated at 900°C and 1000°C. Runs at 1000°C shows a consistently higher weight increase than those at 900°C. Sample batches treated at 1000°C for 20 minutes showed approximately the same weight increase as sample batches treated at 900°C for 160 minutes.

proxy for initial surface area. Being that quartz is such a stable and nonreactive material (as mentioned in section 2.1.6), one would not expect diffusion of carbon into the solid quartz. Consequently, any deposited carbon should be deposited on the quartz surface or on previously deposited carbon.

If all experimental runs were performed with highly uniform pellets, all having the same surface-to-weight ratio, the distinction between weight and surface area would be of less an importance. However, as showed in table 5.2, the surface-to-weight ratios of the different pellet production batches differed by a factor of almost 1.7 ($0.400\ m^2/g / 0.241\ m^2/g$). Such a variance could result in inconsistent results, even though the pellets were exposed to the exact same treatments.

On the assumption that initial surface area is the main qualifier for predicting weight increase at a given temperature, a revision of figure 6.2 was made. By combining initial weight data from table 5.1 with surface-to-weight ratios displayed in table 5.2, a set of recalculated values was produced - now giving the relation between deposited mass and initial surface area. Based on the revised values (table 6.1), two composite charts were produced, each displaying the original values along with the recalculated values. These charts can be seen in figures 6.3 and 6.4, for the samples treated at

Table 6.1: Recalculated values for presenting the ratio of deposited carbon (m_c) to initial sample surface areas (A_q).

900°C				1000°C			
Run no.	Duration [min]	Weight increase	m_c/A_q [g/m^2]	Run no.	Duration [min]	Weight increase	m_c/A_q [g/m^2]
# 09	20	0.07 %	0.0031	# 10	20	1.18 %	0.0489
# 20	20	0.1 %	0.0024	# 11	20	1.38 %	0.0572
# 13	40	0.21 %	0.0088	# 16	40	3.28 %	0.0976
# 15	40	0.46 %	0.0138	# 17	40	3.04 %	0.0759
# 12	80	0.41 %	0.0169	# 19	80	5.68 %	0.1421
# 18	80	0.73 %	0.0182	# 21	80	5.25 %	0.1312
# 08	130	1.16 %	0.0363	# 22	80	5.98 %	0.1495
# 03	160	1.26 %	0.0395	# 05	160	11.08 %	0.3462
# 06	160	1.52 %	0.0475	# 07	160	11.8 %	0.3687
# 02	320	1.53 %	0.0479	# 14	320	19.67 %	0.8163
# 23	320	4.76 %	0.1189				

900°C and 1000°C respectively.

Homogenized data at 900°C

As may be apparent in figure 6.3 (a), there is no overall shift or tendency between the adjusted and unadjusted data at 900°C. However, though not conclusive, there is a slight improvement in the coefficient of determination of the origin-intercepting fitted trend lines, where the adjusted $R'^2_{900°C}$= 0.76 as compared to the initial $R^2_{900°C}$= 0.69. While the coefficient of determination show how well a linear trend line fits the data, it does not indicate if there exists other more suited models for predicting observations.

By making use of a residual plot - which plots how individual observations deviate from a given function - one would be more likely to discover trends in the data. Residuals based on the trend lines of the two data sets were calculated and are shown in figure 6.3 (b). There is no apparent and obvious trend in neither adjusted or unadjusted data.

Homogenized data at 1000°C

Adjusted and unajusted data for 1000°C, along with their respective residuals, are plotted in figure 6.4. There is no discernible difference between the coefficients of determination of the two data sets with their trend at $R'^2_{1000°C}$= $R^2_{1000°C}$= 0.98.

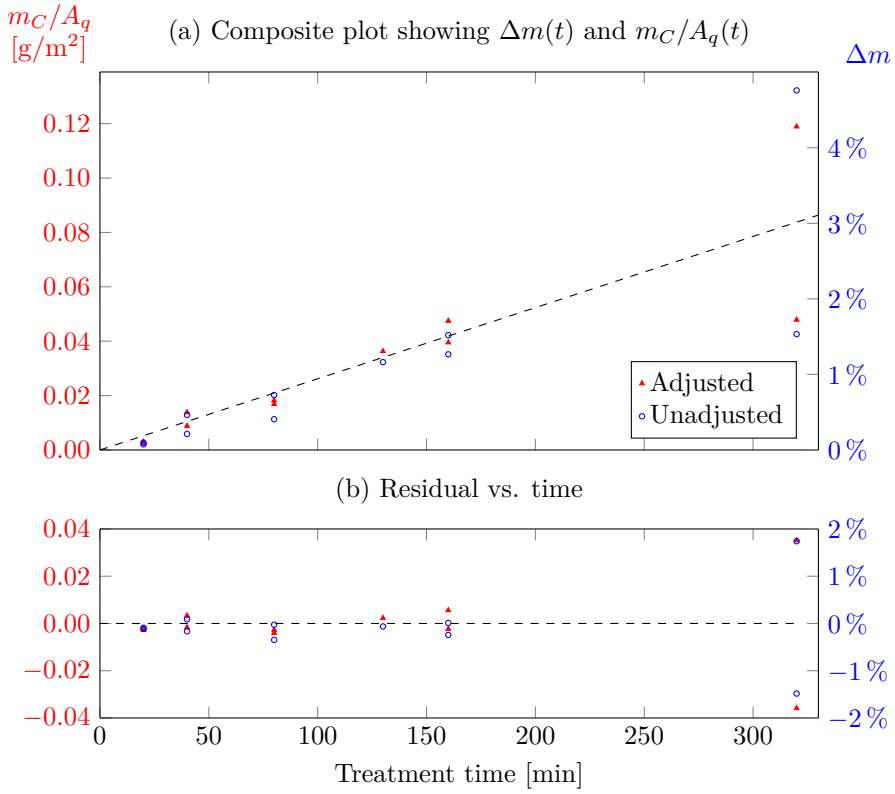

Figure 6.3: The top panel (a) shows adjusted data (left axis, red) plottet as a function of time together with unadjusted data plotted as a function of time (right axis, blue). Microsoft Excel shows coefficients of determination of $R'^2_{900°C}$= 0.76 and $R^2_{900°C}$= 0.69 for the adjusted and unadjusted data respectively. There is no obvious difference in appearance of the two data sets. The bottom panel (b) is a residual vs. time plot, showing deviations from the respective trend lines. There is no apparent change in the tendencies of the data sets, both showing equally erratic behavior around the mean.

A more striking difference between the two sets becomes apparent when looking at the corresponding residual plot - where the adjusted values shows a tendency to slope upwards at higher values while the opposite holds for the unadjusted data.

6.2 Data sets and models

Before proceeding with further analysis, it would be appropriate to decide on which data set one should base further analysis and possible deposition models on. In section 6.1.6 there could not be drawn any definite conclusion as to which set, the homogenized or non-homogenized, that gave the best representation of the data. While the linear fit of the trend line showed higher correlation for the homogenized

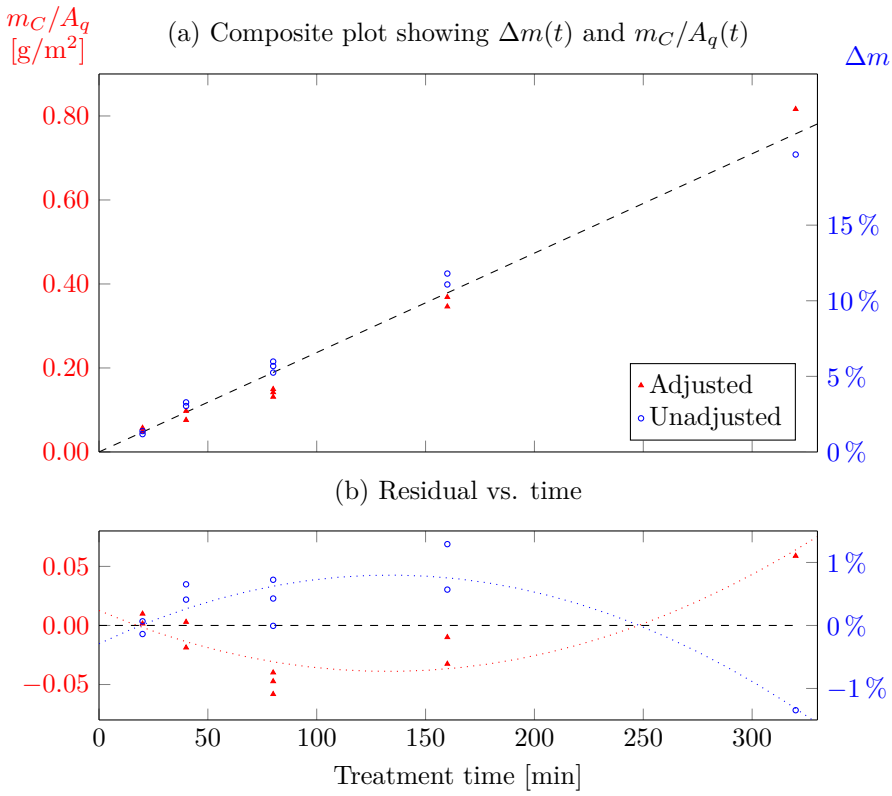

Figure 6.4: The top panel (a) shows adjusted data (left axis, red) plottet as a function of time together with unadjusted data plotted as a function of time (right axis, blue). Microsoft Excel shows coefficients of determination of $R'^2_{1000°C} = R^2_{1000°C} = 0.98$, inidcating an equally good fit. There appears to be a tendency of unadjusted values positioning themselves above the trend line at short time spans and below it at longer treatment durations. The opposite is the case with the adjusted data. Looing at the residual plot (b) these trends become more apparent.

900°C samples, it was not a substantial improvement. And while the residual plots for the 1000°C data sets indicated oppositely curved trends, there was no overall improvement to the general fit.

The fact that there is no obvious and unequivocal improvements when homogenizing the data, could raise doubt of both its validity and usefulness. One main point would be that the deposition process might not be linear, but rather exponential or logarithmic. However, to proceed with the analysis, one should choose the set which is in accord with the basic premise of the research - that carbon deposits on a surface and not on a mass. One question that could be posed, is whether the untreated pellets surface measurements (table 5.2) are representative for the individual production batches, and if weight might be a better predictor for surface

area. Nonetheless, scarce data should be treated as better than no data, and the scientifically based based approach would be to proceed with further analysis based on the homogenized (*or adjusted*) data.

6.2.1 Constant versus transient deposition rates

The linearly fitted trend lines, as shown in figures 6.3 (a) and 6.4 (a), are modeling a situation where carbon deposits at a constant and steady rate. This would suggest that there is no evolution in surface area - neither in the form of increased surface topography or roughness nor the macrostructure geometry - and that the surface reactivity remains constant. In such a system, one would only have to know the weight increase at a point in time to extrapolate for future weight increases, and it could be referred to as *constant*.

A more complex model would account for transient states of deposition, in which deposition rates would transition between being dominated by one factor to another. In the case of the deposition of carbon on quartz pellets, one could imagine an initial state as the exposed quartz surface gets covered with carbon, a second state as the carbon layer grows and possibly a third as geometric factors come into play.

One observations that suggests our system could be more accurately represented by a transient model is that of the specific surface data, which appear clustered around some values. This hints at an initial surface area increase followed by a subsequent stabilization of surface area. An additional indication is given by the residual plot for the 1000°C shown in figure 6.4 (b). Here, the homogenized data show an initial high rate of deposition, followed by lower rates, after which it once again increases and overshoots the linear trend.

Based on the last paragraph, it seems fair to consider if the deposition takes place in transitory stages, each having their own dominant factors. A possible way to approach this problem, would be to distinguish between an initial stage, at which the surface area is increasing, and a following stage, at which the surface area is stable.

Before advancing to further analysis and modeling, it could be valuable to sum up some facts - however mundane or apparent they may be:

- Prior to the deposition of carbon, the pellets have clean quartz surfaces.
- Carbon deposits on both quartz surfaces and previously deposited carbon, as follows by:
    - After methane treatment is initiated, carbon will begin to deposit on the quartz surface.

    - At one point in time, all quartz surfaces will be covered with carbon and any further deposits must take place on previously deposited carbon.

- The surface area increases - i.e. the deposited carbon layers have a greater surface than the initial quartz surface

These facts gives rise to some important questions:

1. How does the methane reactivity vary between carbon and quartz surfaces at different temperatures?
2. Is the methane reactivity of carbon only dependent on temperature, or are there changes as more and more layers get deposited?
3. What is the manner in which deposited carbon correlates to surface area increase?

6.3 Initial stages of deposition

Section 6.2.1 was concluded with some questions relating to the area and the reactivities of the surfaces. The following subsections will try to give some conceivable answers to two of these questions. The possibility of varying methane reactivity of carbon will not be discussed, and it thus assumed to be constant.

The reader should also note that this is a more speculative part of the discussion, hoping to provide some theories as to how the deposition proceeds at the micro-scale.

6.3.1 Effects of different methane reactivities

When assessing possible implication of different methane reactivities in this section, some simplifications are made. Primarily, to attain separate models for surface reactivities and surface roughness, it is assumed that the reactivities does not influence the microscopic surface texture. As the surface gets covered very quickly, one should expect different surface reactivities with methane to manifest themselves at the very early stages of the deposition ($\ll$ 20min).

One could imagine that both quartz and carbon surfaces have two separate and constant reactivities with methane, and that the reactivity of carbon does not change as layers deposit, where only the temperature affects the rate of deposition. The reactivities of quartz and carbon surfaces could be written as $\eta_q(T)$ and $\eta_C(T)$ respectively. The manner in which carbon would initially deposit and subsequently envelop the quartz surface, would be expected to depend on the ratio of these two reactivities.

If one assumes that the deposited carbon layer is so thin that, upon full coverage of the quartz surface, the layer makes no appreciable change in the geometry of the pellet, one could visualize the surface as being flat. Further, assuming that carbon can be approximated as particles which are equally likely to deposit at any angle on previously deposited particles, one could disregard any possible affinity for crystal-like deposition and differences in surface area *or roughness*. Based on these assumptions, three possible scenarios would be:

1. $\eta_q(T) \ll \eta_C(T)$
   Carbon deposits faster on carbon surfaces. As shown in figure 6.5 (a), one would initially expect dispersed occurrences of hemispherical carbon on the quartz surface. Deposition would primarily take place on previously deposited carbon, and successive deposits would lead to a radial growth (figure 6.5 (b)). As the hemispheres grow, the exposed surface area would increase and one should expect an increase in deposition rate. At some point, the growing hemispheres starts to intersect and the surface area growth rate falls off. Finally one reaches a maximum surface area, after which further deposits evens out the bumpy surface and a final carbon surface area that approaches that of the initial quartz surface ($A_C \to A_q$).
2. $\eta_q(T) \sim \eta_C(T)$
   Carbon deposits equally fast on both carbon and quartz surfaces. Carbon initially gets deposited in a dispersed fashion, and as new layers are added, they reflect the topology of the previously deposited carbon, as seen in figures 6.5 (c) and (d). One would expect no appreciable change in the rate of deposition, as there is little change in overall surface area and the reactivities remain constant and equal.
3. $\eta_q(T) \gg \eta_C(T)$
   Carbon deposits faster on quartz surfaces than carbon surfaces. The initial growth consists of dispersed deposits of carbon on the quartz surface, illustrated in figure 6.5 (e). New deposits occur almost exclusively on the exposed quartz surface, and there is no significant change in thickness of previously deposited carbon layers. As less and less quartz surface is exposed to methane (figure 6.5 (f)), the rate of deposition goes down.

To be able to find hints of this in the data, qualitative sketches of individual deposition rates along with projections of deposited carbon mass were produced. The sketches, which are based on the assumptions made for scenarios 1-3, are shown in figure 6.6. A conclusion of the sketches is that the scenarios would be manifest in quite different weight increase curves as a function of time. Specifically:

– $\eta_q(T) \ll \eta_C(T)$ would show a slow initial weight increase, after which deposition

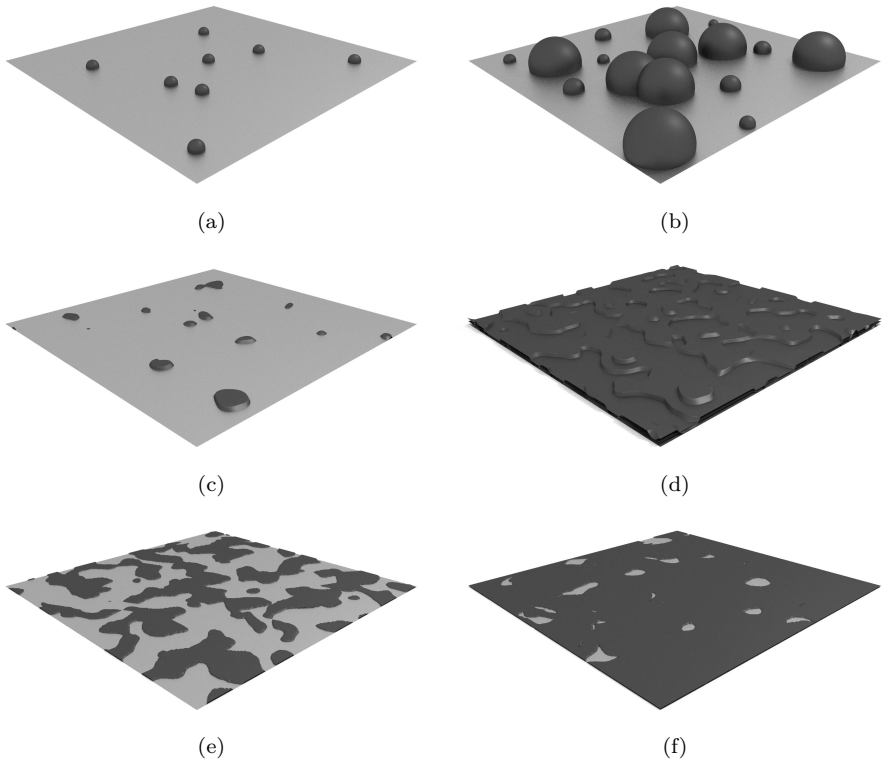

Figure 6.5: Different ratios of the surface reactivities of carbon ($\eta_C(T)$) and quartz ($\eta_q(T)$) with methane gas, would result in different surface topographies. When $\eta_q(T) \ll \eta_C(T)$ the deposition should grow radially from any initial deposits, expanding its surface area and increasing the rate of reaction (a - b). Finlly, the growing hemispheres would start to collide, and as deposition proceeds, the surface area will begin to fall and $A_C(t \gg t_0) \to A_q$. $\eta_q(T) \sim \eta_C(T)$ would give an indiscriminate deposition of carbon, and neither rate nor topography would change appreciably as more carbon gets deposited (c - d). When $\eta_q(T) \sim \eta_C(T)$, carbon primarily deposits on exposed quartz surfaces. As deposition proceeds, all quartz surfaces get covered (e - f) before any substantial growth of the carbon layers take place. As quartz surfaces get enveloped in carbon the deposition rate reduces.

would increase and approach a steady rate(an overshoot before leveling of should be expected, and would depend on the abundance and distribution of radially expanding hemispheres).

– $\eta_q(T) \sim \eta_C(T)$ would show a linear weight increase, in accord with the earlier fitted trend lines.

– $\eta_q(T) \gg \eta_C(T)$ would show a high initial weight increase, after which the deposition rate decreases and reaches a steady state.

6.3.2 Surface texture

One important assumption made in section 6.3.1, is that of no significant increase in surface roughness. All three scenarios were based on the premise that the developing carbon surface area would approach that of the initial quartz surface ($A_C \to A_q$). However, as discussed in previous sections and seen in table 5.2, all treated samples displayed definite increases in surface area. Based on this, a review of the premises set in section 6.3.1 is warranted.

Two graphs, displaying the ratio of final surface area to both initial surface area and deposited carbon mass, are shown in figure 6.8. While there only were surface analysis available for a selection of 11 samples, 4 of which from the 1000°C series and 7 from the °C series, the graphs exhibit some interesting trends.

A surprising result is that total surface area increase is equal for two of the samples at 1000°C, despite having been exposed to methane for vastly different durations (20 vs. 320 minutes) and gaining substantially different masses of carbon. While all four data points at 1000°C do show a large increase in surface area, something that suggests a high initial increase, the ensemble is so inconsistent that it does not provide any clear answers.

The seven observations at 900°C show more consistent trends, where there seem to be a an initial high rate of surface increase after which the rate drops off and the surface area remains fairly stable. The left panel in figure 6.8, where surface increase is plotted as a function of gained mass, also show two of samples treated at 1000°C lining up together with the 900°C samples - an observation that suggest a surface roughness that primarily is a function of weight increase and not temperature. To emphasize this, a dashed black line has been added to the left panel. The line was produced by fitting a Michaelis-Menten-like function to the data:

$$f(x) = \frac{x}{a + b \cdot x} \tag{6.1}$$

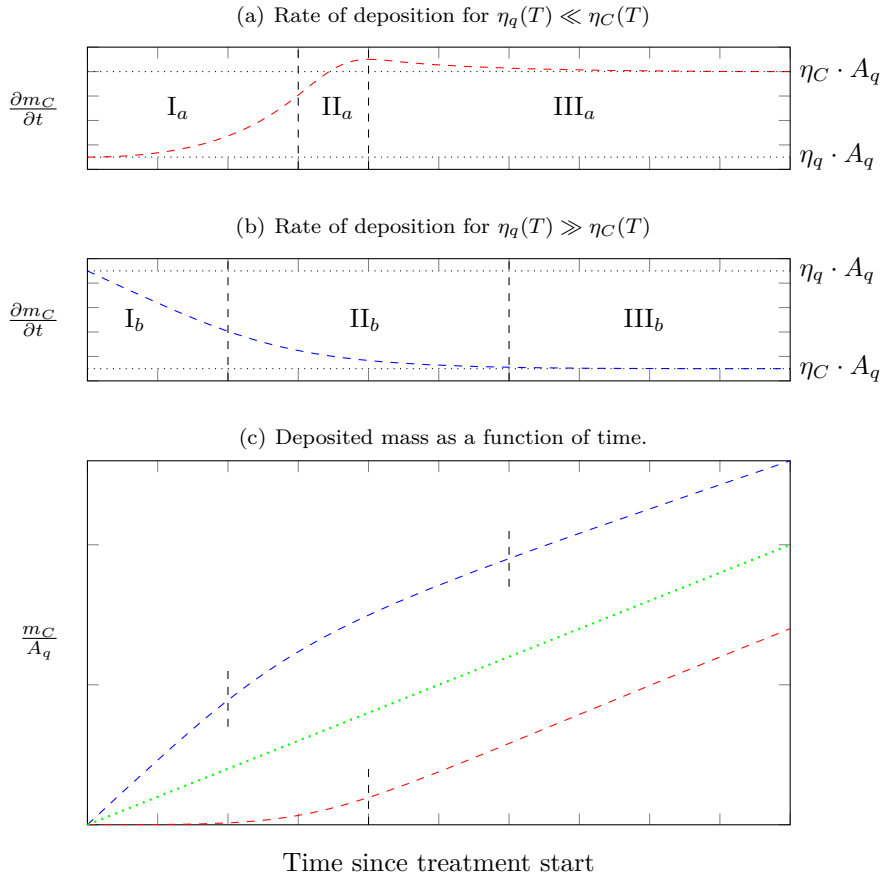

Figure 6.6: Qualitatively sketched deposition rates for different ratios of η (a, b) and projected weight increase in relation to initial surface area (c). If carbon exhibits the larger reactivity with methane (a), one would expect an exponential growth (I_a) period, where deposits develop as hemispheres and, by radial growth, increases their surface area. The expanding hemispheres starts to coalesce and the growth rate of the carbon surface area falls off (II_a). The carbon surface reaches its maximum, and moves into a region (III_a) where A_C slowly falls and approaces A_q. In a situation where quartz exhibits a higher reactivity (b), the quart surface will display an initial linear loss of surface (I_b). As the surface gets covered by carbon, one moves into a region (II_b) with diminishing quartz surface, until all quartz is enveloped in carbon and reaches steady state (III_b). The remaining scenario is that of similar reactivities for carbon and quartz, a situation where growth would be linear, and is only illustrated by the green line in (c).

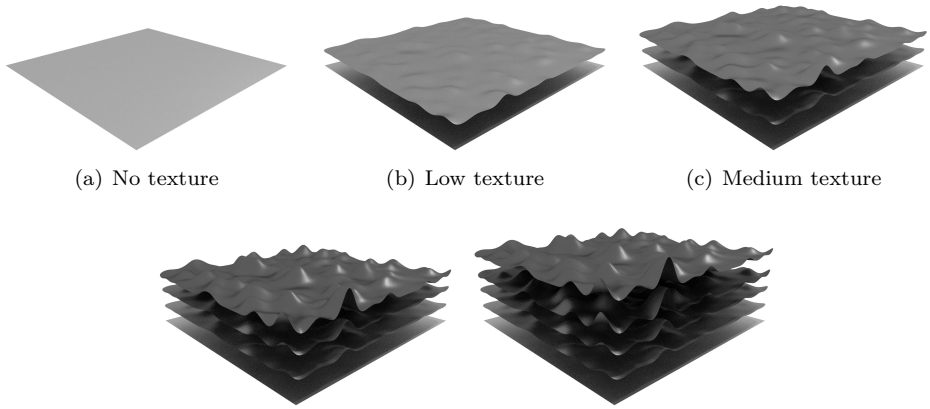

(a) No texture (b) Low texture (c) Medium texture

(d) Maximum texture (e) No further texture change

Figure 6.7: An initial surface without texture (a) gets an increased texture as subsequent layers of carbon deposits (b - c), before finally reaching a maximum roughness (d) after which there is no change in surface area as addition layers accumulate (e).

The strongest conclusion that can be drawn from the data, is that there is a definite increase in surface area as time passes. This increase initially starts at a high rate. After time passes and carbon deposits, this rate seem to drop to 0 or a significantly lower value. Such a scenario is depicted in figure 6.7, where the carbon layer initially adds to the surface texture before leveling out at a specific surface roughness.

When looking at the relationship of the difference in initial and final surface area (ΔA) to deposited mass (m_C), the surface data for 900°C as well as two data points at 1000°C show a remarkably high degree of agreement with a Michaelis-Menten function based on deposited mass - i.e. $\Delta A(m_C) = {}^{m_C}/_{a + bm_C}$ (a, b - fit parameters) serves as a good predictor of surface area. Based on this function, there seem to be little evolution of surface texture after 0.05 - 0.10 g/m^2. Similar considerations for the relationship between ΔA and treatment duration does not produce an equally strong match.

Provided that deposited mass is the best proxy for surface area, further manipulations can be performed with the data to indicate at which time this trend diminishes for the respective temperature treatments, and thus a progress into a new transient deposition state.

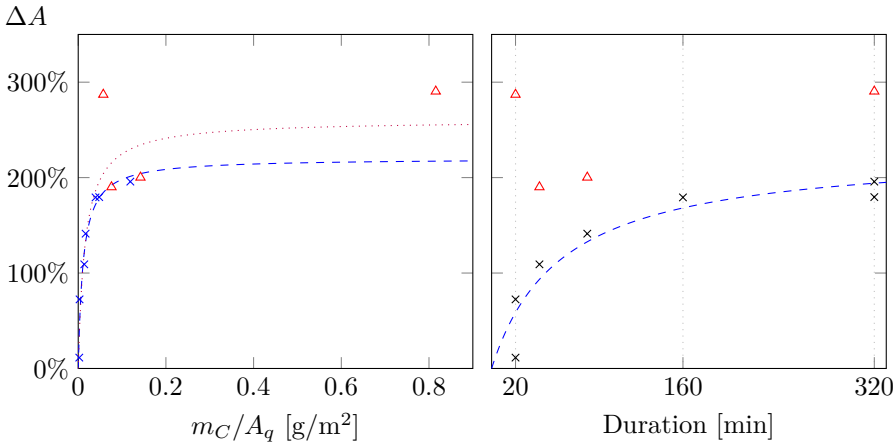

Figure 6.8: The difference in surface area (ΔA) as a function of weight increase [left panel] and treatment duration [right panel], of which both indicate an initial quick surface increase. The red triangles data at 1000°C and the blue crosses data at 900°C. A Michaelis-Menten-like equation (eq. 6.1, a=$5.1{\cdot}10^{-3}$,b=0.45), which is used to describe an almost linear growth followed by convergence towards a given value, has been fitted to the 900°C data in the left panel (dashed blue). The function shows a coefficient of determination of $R^2 = 0.94$. If the function is fitted to all the data points as illustrated with the purple dotted curve, including those at 1000°C, the correlation falls to $R^2 = 0.81$, and other combinations of the two sets do not perform as well as if based only on the 900°C data. In the right panel, the function has also been fitted to the data at 900°C and shown with a blue dashed line, giving $R^2 = 0.89$ (eq. 6.1, a=25.4,b=0.44).

6.3.3 Impact of deposition models

The models presented in the previous two sections provided possible mechanisms that influence the deposition process. One obvious difference between the two, is that differences in methane reactivities would produce no final difference in surface area, while the evolution of texture would produce a higher surface area. The timescales at which the different mechanisms would work also differ, and while different methane reactivities would be manifested en the period before the surface is covered in carbon, surface texture would evolve as addition layers of carbon deposit.

Based on the fact that the shortest treatment duration in this study was 20 minutes, a duration at which both temperature series would have had total surface coverage of methane, this mechanism is hard to verify with the available data.

The model of surface texture would be more likely to show up in the data, as it evolves through the growth of carbon layers. Since the model had a promising correlations with the experiments at 900°C, as well as two of the points at 1000°C, it could be worth looking into in future research.

While being of more a speculative character, the previous sections have presented

some possible mechanisms that influence the early stages of carbon deposition from methane on quartz. Moreover, some promising correlations have been seen for the evolution of surface. To complete this line of reasoning, a deposition that is transitioning between stages, the following section will provide some brief thoughts as to what may be influencing the later stages of deposition.

6.4 Intermediate stage of deposition

Briefly touched upon in section 5.1, the longest treatment duration at 1000°C showed a great deal of agglomeration. As a result of this, it was concluded that this sample was less likely to be representative of the time period following the surface increase, and it was accordingly excluded.

As discussed in section 6.3.2, there seemed to be little change to the surface texture passed an initial deposition of 0.05 - 0.1 g/m^2. By looking at figures 6.3 and 6.4, on can see that this interval is reached after approximately 170 minutes for the 900°C series and 20 minutes for the 1000°C series. Assuming that there is little or no change in surface area after these treatment durations, one could look for the presence of other mechanisms which influence deposition past this point, while assuming 0 or constant surface area increase.

I follows from the 900°C data that the scarcity and high variance of the data points beyond 170 minutes makes it unsuited for further discussion. However, for the 1000°C series, all data points are close to or above 0.05 g/m^2, with the lowest being 0.0489 g/m^2 (6.1).

On the assumption of no further texture development, additional deposition would either run at a constant rate as more layers are being added, or at an exponential rate, where the carbon layer thickness becomes so large as to impact the macroscopic geometry of the pellets.

Based on this, both linear and quadratic trend lines were fitted to the data, and in contrast to the analysis made in the subsections of 6.1, the lines were not forced to intersect with the origin. The quadratic trend, although being highly speculative, prooved a nice fit with R^2=99. This could be an indication of an intermediate stage, in which increase in the geometry of the particle, as additional layers of carbon get added, is the main controlling mechanism.

6.4.1 Summary

As shown in the, there exist possibilities of a controlling mechanism of the deposition being divided in mainly two parts, initial surface texture development and an intermediate stage controlled by the growing geometry of the particle.

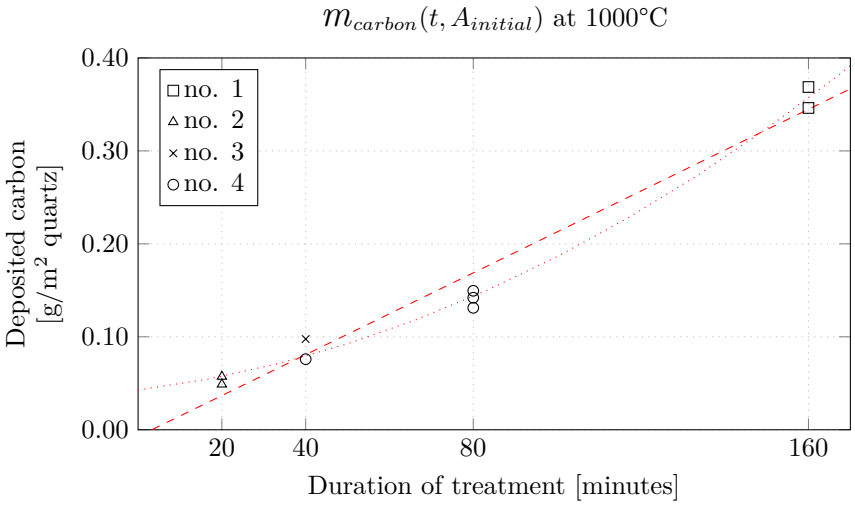

Figure 6.9: A linear and a quadratic function has been fitted to the data of the 1000°C data. The linear fit seem to give a poor representation of the deposition process. The quadratic fit ($8.8{\cdot}10^{-6} \cdot x^2 + 5.54 \cdot 10^{-4} + 0.04$) showed a coefficient of determination of R^2=0.99. As it becomes exceedingly likely to have good data as one adds factors, this should only be viewed as a speculation. But if it were a representation of a real mechanism in the deposition process, it could represent the geometric growth of the particle as new layers of carbon get added.

These latter sections have been based largely on speculation. This means that the reader should not take these thoughts as conclusive, but rather as suggestions and possible further research.

6.5 Error sources

The following sections will provide some short comments on error sources and their impact on the experiments.

6.5.1 Handling of samples

The handling of samples between initial and final weighing could contribute to the loss of sample mass. Pellets lost from the crucible unnoticed and deposits falling into the crucible, such as noted on the deposited carbon flakes in section 4.2.12, are examples of such errors.

While one can not exclude that these factors played a role in individual treatments, one should not expect such occurrences to impact the overall observations from this study. In addition, the loss of pellets, as discussed in section 6.1.4, were likely of little significance, much as a result of the sample sizes weighing in excess of 40 g.

A final indicator of losses through the entire treatment process, from initial to final weighing, is sample # 02. As mentioned in section 5.1, this sample was treated at 700°C for 160 minutes without showing any visual signs of deposition and having a weight loss of 0.07 %. Assuming there were no deposition of carbon, this experiment serves as an indicator of what losses one might expect during a typical treatment.

6.5.2 Temperature stability

The matter of temperature stability has largely been commented on in section 6.1.4, where it was concluded that there were no significant deviations from from the desired temperatures throughout the different experimental runs.

6.5.3 Gas flow during treatment

Since the samples were treated with high flow rates of gas, there could be an issue with particulates being ejected from the sample crucible. In light of the discussion on lost pellets in section 6.1.4 and the fairly small weight loss in experiment # 02 (as discussed in section 6.5.1), gas flow should have no considerable impact on the experiments.

As noted in section 5.1, pellets treated at 1000°C were observed to fuse together. While this speaks of the amount of carbon that must have deposited, one should also expect this to lead channeling of gas through the sample batch. This could contribute individual pellets being exposed to different levels of methane gas as well as impact the thermal profile within the sample crucible. The final impact of channeling is hard to assess. However, the vast majority of experiments had little or no agglomeration of pellets, and with the exception of longest run at 1000°C this has been assumed to be a minor issue.

One of the samples exposed to an irregular treatment, run # 23, showed a high weigh increase compared to the similar run # 02. While the total exposure time were the same for the two runs, sample # 23 had several intermittent treatments with argon gas. Both increased pressure and intermittent treatments with argon could have had an impact on the total weight gain, and one should not rely on this sample in any definite conclusions.

6.5.4 Measurement errors

Measurement errors as a result of errors of the weight scale has not been considered an issue in these experiments, and constant deviations should not play a role as the same weight scale was used throughout the experiments.

6.5.5 Post-treatment surface change

A factor that has not been given great attention in this work, is the behavior of the deposited surfaces post-treatment. During the cooling phase, the deposited layer of carbon would be exposed to high temperatures. One could imagine that this affects the structure of the individual layers of carbon, possibly leading to a restructuring and recombination of layers.

An additional issue relates to the carbon surfaces and the possibility of oxidation as the samples are removed from the furnace, weighed, bagged and subsequently stored.

As a result of these mainly unknown factors, one should not place a too high certainty on the specific surface area measurements. This should play no major role on their use in affirming that there is a surface increase, but it could be more of an issue it relates to observations made from figure 6.8.

Chapter 7
Recommendations for Future Research

The author would like to provide some thoughts on possible future research.

7.1 Gas composition

One of the decisions made at the outset of this study was to limit the number of parameters present during the experiments - a decision that led to a treatment with only high purity methane at a very high flow rate. While such a decision reduces the number of factors that could influence the experimental results, giving a higher probability of consistent results, this is far from a real world situation.

For the cracking of methane to be applicable on an industrial scale, one would need a high factor of conversion. This would introduce large volumes of hydrogen gas into the system, where for every methane molecule cracking, there would be two hydrogen molecules produced.

If made with the goal of implementing the process discussed in this thesis on an industrial scale, future studies should certainly consider adding hydrogen to the mix.

7.2 Equipment

As briefly mentioned in section 4.3, there exists equipment which could help supplement the observations made in this study, one of which is the Tapered Element Oscillating Microbalance(TEOM). This is an apparatus that provides a continual stream of highly accurate weight data throughout an experiment, an ability that could help uncover when and how different reactions takes place during the deposition process.

To better understand the processes taking place during the carbon deposition on quartz, future research should consider taking use of alternative techniques, such as the TEOM or off-gas monitoring systems. This could provide a more complete

picture of how the process progresses. Equipment that could give *in situ* observations of the deposited carbon, if it exists, could also add to our knowledge.

7.3 Cycling of treatments

One peculiarity that was noted in section 6.5.3, as one sample being exposed to intermittent periods of argon showed a substantially larger weight increase than a similar sample which had a continual treatment.

While this observation may be a result of higher pressure or other occurrences, the author suggest performing new experiments with intermittent argon treatment, so as to uncover if this was a one off or possibly another mechanism which comes into play.

Chapter 8
Conclusion

8.1 Concluding remarks

This work has shown that pure methane, when exposed to quartz at a temperatures of 900°C and 1000°C, cracks and deposits carbon at a near constant rate.

The deposition rates for the individual temperature levels were shown to differ by a factor of approximately 7, where experiments at 1000°C showed the highest rate of deposition and those at 900°C the lowest.

The surfaces of the samples showed a definite increase after the treatment. While not definite, there were signs that surface area could be a function of deposited carbon mass.

There were not observed any weight increase on the sample treated at 700°C, and only small amounts on the sample at 800°C, indicating a cut-off temperature for the reaction in this interval.

Bibliography

[1] U.S. Geological Survey. Mineral Commodity Summaries (1996-2014): Silicon. Technical report, U. S. Geological Survey.

[2] J K Tuset, A Schei, and H Tveit. *Production of High Silicon Alloys*. Tapir Forlag, 1998.

[3] European Commission. Reference Document on Best Available Techniques in the Non Ferrous Metals Industries. Technical Report December, 2001.

[4] A. A. Yaroshevsky. Abundances of chemical elements in the Earth's crust. *Geochemistry International*, 44(1):48–55, January 2006.

[5] Bodil Monsen, Leiv Kolbeinsen, Steinar Prytz, Viktor Myrvå gnes, and Kai Tang. Possible Use of Natural Gas for Silicon or Ferrosilicon Production. In *Possible use of natural gas for silicon or ferrosilicon production. Proceedings of the thirteenth international ferroalloys congress. Efficient Technologies in Ferroalloy Industry.*, volume 1, pages 467–478. Almaty, Kazakhstan: P. Dipner., 2013.

[6] Svein Stölen and Tor Grande. *Chemical Thermodynamics of Materials: Macroscopic and Microscopic Aspects*. 2004.

[7] Harold Johann Thomas Ellingham. Transactions and communications. *Journal of the Society of Chemical Industry*, 63(5):125–133, 1944.

[8] F. D. Richardson and J. H. E. Jeffes. The Thermodynamics of Substances of Interest in Iron and Steel Making from 0°C to 2400°C: I-Oxides. *The Journal of the Iron and Steel Institute*, 160:261, 1948.

[9] S.Y. Lee, N. Mettlach, N. Nguyen, Y.M. Sun, and J.M. White. Copper oxide reduction through vacuum annealing. *Applied Surface Science*, 206(1-4):102–109, February 2003.

[10] Elena Dal Martello. *Impurity distribution and reduction behaviour of quartz in the production of high purity silicon*. PhD thesis, Norwegian University of Science and Technology, 2012.

[11] Edin Henrik Myrhaug and Halvard Tveit. Material Balances Of Trace Elements In The Ferrosilicon And Silicon Processes. In *Electric furnace conference proceedings*. Association for Iron and Steel Technology, 2000.

[12] Ashraf M. Amin, Eric Croiset, and William Epling. Review of methane catalytic cracking for hydrogen production. *International Journal of Hydrogen Energy*, 36 (4):2904–2935, February 2011.

[13] R MOLINER, I SUELVES, M LAZARO, and O MORENO. Thermocatalytic decomposition of methane over activated carbons: influence of textural properties and surface chemistry. *International Journal of Hydrogen Energy*, 30(3):293–300, March 2005.

[14] I. Suelves, M.J. Lázaro, R. Moliner, J.L. Pinilla, and H. Cubero. Hydrogen production by methane decarbonization: Carbonaceous catalysts. *International Journal of Hydrogen Energy*, 32(15):3320–3326, October 2007.

[15] M.J. Lázaro, J.L. Pinilla, I. Suelves, and R. Moliner. Study of the deactivation mechanism of carbon blacks used in methane decomposition. *International Journal of Hydrogen Energy*, 33(15):4104–4111, August 2008.

[16] Thomas Battle, Urvashi Srivastava, John Kopfle, Robert Hunter, and James McClelland. *Treatise on Process Metallurgy*. Elsevier, 2014.

[17] Oleg Ostrovski and Guangqing Zhang. Reduction and carburization of metal oxides by methane-containing gas. *AIChE Journal*, 52(1):300–310, 2006.

[18] Herbert J. Fromm and Mark Hargrove. *Essentials of Biochemistry*. 2012.

[19] RF Egerton. *Physical principles of electron microscopy*. Springer, 2005.

[20] Stephen Brunauer, P H Emmett, and Edward Teller. Adsorption of Gases in Multimolecular Layers. *Journal of the American Chemical Society*, 60(2):309–319, 1938.